Sb(V)dihalide Corroles: Efficient Singlet Oxygen Photosensitisers

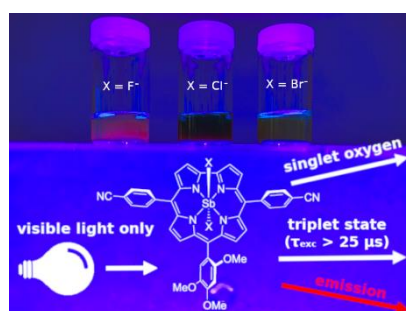Volkan Caliskanyürek [a], Simon Eulberg [b], Oliver Lange [a], Martin Bröring [*b] and Stefanie Tschierlei [*a]

a   Department of Energy Conversion, Institute of Physical and Theoretical Chemistry, Technische Universität Braunschweig, Rebenring 31, 38106 Braunschweig, Germany
E-mail: s.tschierlei@tu-bs.de
b   Institute of Inorganic and Analytical Chemistry, Technische Universität Braunschweig, Hagenring 30, 38106 Braunschweig, Germany
E-Mail: m.broering@tu-bs.de

Table of Content

1 Experimental Details

NMR spectroscopy. ^{1}H-, ^{13}C- and ^{19}F-NMR spectra were obtained on a Bruker Avance II 300, a Bruker Avance III HD 300N, a Bruker Avance III HD 500 or a Bruker Avance II 600 spectrometer at room temperature. Chemical shifts (δ) are given in ppm relative to TMS and referenced against residual protio solvent resonances, or $CFCl_3$.

Mass spectrometry. Mass spectra were recorded on a Finnigan LCQ-Deca instrument with electrospray source in positive mode. All samples were measured in acetonitrile. m/z values are given for the most abundant isotopes only.

Steady-state absorption spectroscopy. A JASCO V-770 spectrophotometer was used to record steady-state UV/vis absorption spectra. All samples were measured in solution of dichloromethane or deuterated chloroform in a standard 1 cm quartz glass cuvette. The solvent selected in each case served as a reference. The data interval was set to 1 nm and a continuous scan rate of 400 nm/min was chosen. The bandwidths were set to 1 nm in the UV/vis region.

Steady-state emission spectroscopy and quantum yield determination. Steady-state visible emission measurements were recorded by using a Horiba FluoroMax Plus and a R928P photon counting PMT as detector. Unless stated otherwise, all measurements were carried out under inert conditions using Argon as inert gas. Optical densities were set to 0.1 to prohibit self-quenching/reabsorption. For quantum yield determination, [Ru(bpy)$_3$]Cl$_2$ in dichloromethane was used as reference (ϕ_r=0.10, inert).[1] The error of quantum yields is estimated to be ±10%. Eq. S1 was used to calculate the quantum yield.[2]

$$\varphi_r = \varphi_{r,ref} * \left(\frac{A_{ref} \cdot \int \mathrm{Em_{sample}}}{A_{sample} \cdot \int \mathrm{Em_{ref}}} \right) \qquad \text{eq. S1}$$

Steady-state infrared emission measurements were recorded by using a Horiba FluoroMax Plus and a DSS-IGA020L InGaAs solid state detector. The detector was cooled with liquid nitrogen for at least 30 minutes prior to each measurement. Optical densities were set to 0.1 for the excitation wavelengths respectively. In the case of the singlet oxygen emission (at ~1278 nm) studies, air saturated dichloromethane or deuterated chloroform ($CDCl_3$) were used as solvents and the excitation wavelength λ_{exc} was set to match the Soret-band λ_{Soret}. Deuterated chloroform has a significantly lower singlet oxygen deactivation rate τ_d when compared to dichloromethane and chloroform.[3] No other measurements have been carried out in deuterated chloroform due to cost and energy factors as well as a lack of reference values.

Singlet oxygen quantum yield (φ_{1O2}) was determined through eq. S2. As reference, Perinaphtenone (PN, assuming φ_{1O2} = 1 in aerated dichloromethane) was used and the error is estimated to be about ±10%.[4,5]

$$\varphi_{1O_2} = \varphi_{1O_2} \cdot \left(\frac{A_{ref} \cdot \int \mathrm{Em_{sample}}}{A_{sample} \cdot \int \mathrm{Em_{ref}}} \right) \qquad \text{eq. S2}$$

Time-dependent *in situ* absorption spectroscopy. *In situ* measurements of time-dependent UV/vis absorption spectra during (photo-)chemical reactions were recorded with an Avantes StarLine AvaSpec-

ULS2048CL-EVO-RS spectrophotometer connected to an Avantes AvaLight-DH-S-BAL light source *via* fiber-optic cables. The integration time was set to 1.25 ms and spectrum was averaged over 100 measurements.

Photooxidation of 2,5-diphenylfuran (DPF). Firstly, three solutions were prepared, yielding a $1.9 \cdot 10^{-4}$ M solution of DPF (solution A), a $1.9 \cdot 10^{-5}$ M solution of DPF (solution B) and a $1.9 \cdot 10^{-6}$ M solution of PS (solution C) respectively. Afterwards, 1.2 mL of B and C were transferred inside a cuvette. A micro stirring bar was added and the cuvette was stirred at 800 rpm. A Cold Light Source LED3 by StarLight Opto-Electronics was used to irradiate the sample (visible light only) and an the above mentioned Avantes StarLine Setup was used to measure the *in situ* UV/vis spectra. During recycle experiments, 120 μL of solution A was added to the cuvette after 1 h.

Nanosecond transient absorption spectroscopy. A pulsed Nd:YAG laser (Quantel Q-smart) with an output centred at 355 nm was used to excite the sample. The pulse duration was approximately 6 ns using a repetition rate of 10 Hz. Notch filters with a central wavelength of 355 ± 2 nm (FWHM = 10 ± 2 nm) were used to ensure monochromatic irradiation of the sample. The laser power was set to ~3 mJ per pulse in front of the sample. The transient absorption signals were recorded by a LP980-K from Edinburgh Instruments, with a 150 W Xenon lamp as probe lamp, containing a Hamamatsu R928P photomultiplier tube (PMT). The investigated samples were prepared with an optical density of 0.3 in inert, dry dichloromethane and placed in a gas-tight 10 mm quartz cuvette.

Time-resolved emission measurements. Three-dimensional characterisation of a sample's emission intensity with respect to time and wavelength was conducted with a streak camera. Excitation was conducted with a 373 nm pulsed laser diode (M10306-27, pulse width: ~42 ps) at optical densities of 0.1 in inert dichloromethane. Streak images were recorded using a HAMAMATSU Universal Streak Camera C10910-01 in conjunction with a Kymera 328i-A spectrograph by ANDOR at 21 °C. The power output of the laser diode entering the cuvette was 44.4 μW. The repetition rate of 4 MHz and the triggering was controlled externally through a PC coupled to the C10196 light pulse control unit. Emission was recorded perpendicular to the excitation beam and was directed into the spectrograph with two plano convex lenses through an adjustable slit (**1**: 500 μm; **2** and **3**: 400 μm) onto a diffraction grating (50 l/mm, blaze: 600 nm).

Computational Details. All calculations have been carried out with density functional theory (DFT) in ORCA (version 5.0.4) which was parallelised with OpenMPI (version 4.1.1).[6] The M06 functional has been used with the def2-TZVPP basis set.[7] To account for the grid sensitivity of the Minnesota functionals the grid was set to "DEFGRID3" and SCF convergence criteria were set to the "TightSCF" keyword for all computations. The D3zero dispersion correction was included in all computations.[8] The resolution of identity for the Coulomb terms coupled with the chain of spheres algorithm (RIJCOSX) was utilized with the def2/J auxiliary basis set to speed up computations.[9]

The ground state structures (multiplicity: 1, charge: 0) of **1**, **2** and **3** and the lowest triplet state of **1** (multiplicity: 3, charge: 0) were optimized within the implicit solvent model CPCM with dichloromethane as the chosen implicit solvent.[10] Harmonic analytical frequencies at the identical level of theory confirmed all structures to be minimum structures on the potential energy surfaces as no imaginary frequencies were found.[11] A single-point energy calculation at the same level of theory was launched to determine the molecular orbital coefficients.

Excitation energies of the first 150 electronic transitions were obtained on the electronic singlet ground state minimum structures with Tamm-Dancoff time-dependent DFT.[12] Gauss-broadened stick spectra (FWHM = 2000 cm^{-1}) were created with the orca_mapspc program, manually shifted higher by 40 nm and visualized in R. Molecular orbitals (isosurface values ±0.025) and difference density plots (isosurface values ±0.0075) of excitations with an oscillator strength > 0.01 were created in ChimeraX with the SEQCROW plugin.[13]

2 Synthesis and General Characterisation

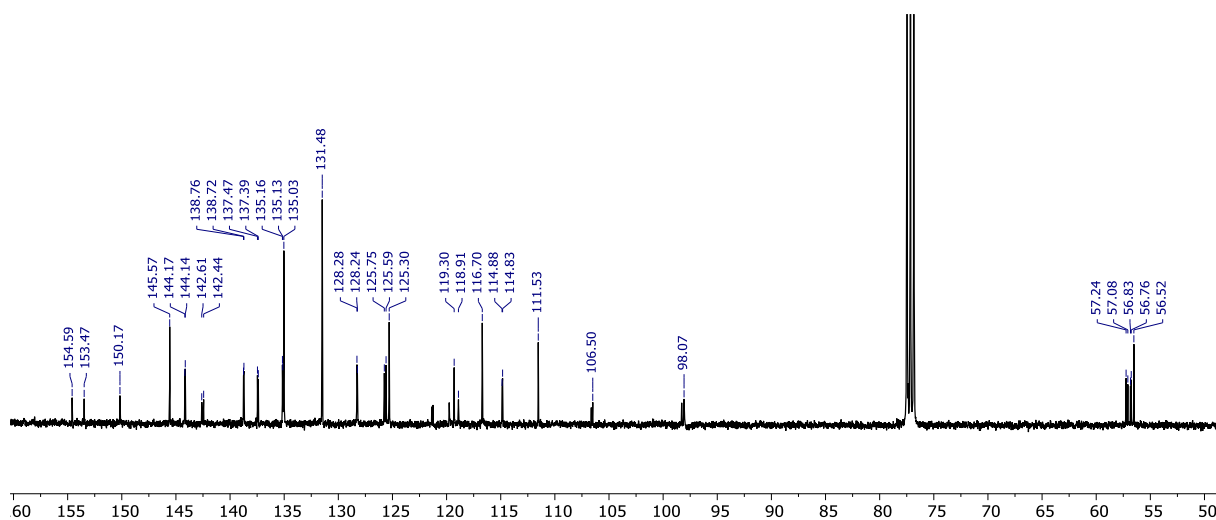**5,15-Di(4-cyanophenyl)-10-(2,4,5-trimethoxyphenyl)-corrolatoantimon(III)**

Corrole (193 mg, 0.29 mmol, 1 eq.) and $SbCl_3$ (198 mg, 0.87 mmol, 3 eq.) are dissolved in pyridine (30 mL) and stirred for 60 min at 100°C until a colour change to brownish-yellow is observed. The solvent is removed in vacuo at 60°C. Subsequently, a column chromatographic purification on silica is carried out with a mixture of dichloromethane/methanol (150:1). After recrystallisation in dichloromethane/n-hexane and drying in high vacuum, a brownish-yellow crystalline material (145 mg, 0.18 mmol, 64%) is isolated.

^{1}H NMR (400 MHz, $CDCl_3$) δ = 9.22 (dd, J = 4.1 Hz, 1.7 Hz, 4H, *β-H*), 9.02 (d, J = 4.3 Hz, 2H, *β-H*), 9.01 (d, J = 4.2 Hz, 2H, *β-H*), 8.79 (d, J = 4.7 Hz, 2H, *β-H*), 8.77 (d, J = 4.7 Hz, 2H, *β-H*), 8.72 (d, J = 4.1 Hz, 4H, *β-H*), 8.36 (br. s, 8H, 5,15-(Ph-*H*)), 8.08 (d, J = 8.5 Hz, 8H, 5,15-(Ph-*H*)), 7.72 (s, 1H, 10-(Ph-*H*)), 7.31 (s, 1H, 10-(Ph-*H*)), 7.04 (s, 1H, 10-(Ph-*H*)) 6.96 (s, 1H, 10-(Ph-*H*)), 4.21 (s, 3H, 10-(OC*H₃*)), 4.19 (s, 3H, 10-(OC*H₃*)), 3.98 (s, 3H, 10-(OC*H₃*)), 3.83 (s, 3H, 10-(OC*H₃*)), 3.72 (s, 3H, 10-(OC*H₃*)),3.38 (s, 3H, 10-(OC*H₃*)).
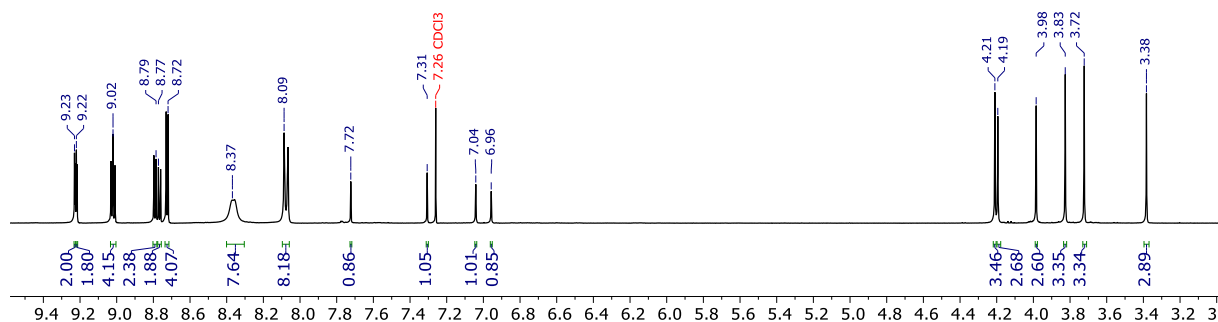
Figure S1. ^{1}H NMR spectrum of 5,15-Di(4-cyanophenyl)-10-(2,4,5-trimethoxyphenyl)-corrolatoantimon(III) in deuterated chloroform ($CDCl_3$).

^{13}C NMR (101 MHz, $CDCl_3$) δ = 154.6 (s, 1C, 10-(Ph*C*OCH₃)),153.5 (s, 1C, 10-(Ph*C*OCH₃)), 150.2 (s, 2C, 10-(Ph*C*OCH₃)), 145.6 (s, 4C, 5,15-(*C*N-Ph)), 144.2 (s, 2C, α-*C*), 144.1 (s, 2C, α-*C*), 142.6 (s, 1C, 10-(Ph*C*OCH₃)), 142.4 (s, 1C, 10-(Ph*C*OCH₃)), 138.8 (s, 2C, α-*C*), 138.7 (s, 2C, α-*C*), 137.5 (s, 2C, α-*C*), 137.4 (s, 2C, α-*C*), 135.2 (s, 2C, α-*C*), 135.1 (s, 2C, α-*C*), 135.0 (s, 8C, 5,15-(*o*-Ph*C*)), 131.5 (s, 8C, 5,15-(*m*-Ph*C*)), 128.2 (s, 2C, *β-C*), 128.2 (s, 2C, *β-C*), 125.8 (s, 2C, *β-C*), 125.6 (s, 2C, *β-C*),125.3 (s, 4C, *β-C*), 121.4 (s, 1C, 10-(*ipso*-Ph*C*)), 121.3 (s, 1C, 10-(*ipso*-Ph*C*)), 119.8 (s, 1C, 10-(*o*-Ph*C*H)), 119.3 (s, 4C, 5,15-(*ipso*-Ph*C*)), 118.9 (s, 1C, 10-(*o*-Ph*C*H)),116.7 (s, 4C, *β-C*), 114.9 (s, 2C, *meso-C*), 114.8 (s, 2C, *meso-C*), 111.5 (s, 4C, 5,15-(*p*-Ph*C*)), 106.6 (s, 1C, *meso-C*), 106.5 (s, 1C, *meso-C*), 98.3 (s, 1C, 10-(*m*-Ph*C*H)), 98.1 (s, 1C, 10-(*m*-Ph*C*H)), 57.2 (s, 1C, 10-(O*C*H₃)), 57.1 (s, 1C, 10-(O*C*H₃)), 56.8 (s, 2C, 10-(O*C*H₃)), 56.5 (s, 2C, 10-(*p*-O*C*H₃)).
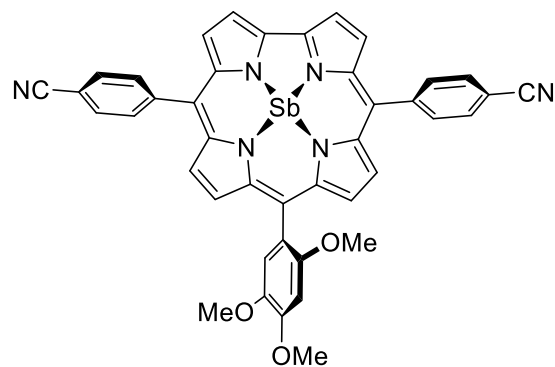
Figure S2. ^{13}C NMR spectrum of 5,15-Di(4-cyanophenyl)-10-(2,4,5-trimethoxyphenyl)-corrolatoantimon(III) in deuterated chloroform (CDCl$_3$).

MS (ESI): m/z = 784 ([M]$^+$), 769 ([M-CH$_3$]$^+$).

UV/vis (Dichloromethane): λ$_{max}$ (ε [L·mol^{-1}·cm^{-1}]) = 446 (80200), 463 (64700), 544 (8500), 572 (7100), 615 (8200), 666 (21400) nm.

**CHN**: Calc. for C$_{42}$H$_{27}$N$_6$O$_3$Sb (in %): C, 64.22; H, 3.46; N, 10.70. Found: C, 64.22; H, 3.67; N, 10.26.

Figure S3. Structure of 5,15-bis(4-cyanophenyl)-10-(2,4,5-trimethoxyphenyl)corrolatoantimon(III).

Di-μ-oxido-bis{5,15-di(4-cyanophenyl)-10-(2,4,5-trimethoxyphenyl)corrolatoantimon(V)}

Antimony(III)corrole (150 mg, 0.19 mmol, 1 eq.) and iodosobenzene (84 mg, 0.38 mmol, 2 eq.) are dissolved in toluene (50 mL) and refluxed at 130°C for 1 h. A colour change from brownish-yellow to greenish-blue is observed. The excess of iodosobenzene is removed by filtration and the solvent is removed in vacuo. After recrystallisation from dichloromethane/n-hexane and drying in high vacuum, a greenish-blue crystalline material (152 mg, 0.19 mmol, quant.) is obtained.

^{1}H NMR (300 MHz, THF-d_8) δ = 8.94 (br. s., 4H, *β-H*), 8.85 (br. s, 4H, *β-H*), 8.60 (br. s, 4H, *β-H*), 8.33 (br. s, 4H, *β-H*), 8.15 (br. s, 8H, 5,15-Ph*H*), 7.99 (br. s, 8H, 5,15-Ph*H*), 7.03 (br. s, 2H, 10-Ph*H*), 6.90 (br. s, 2H, 10-Ph*H*), 4.09 (br. s, 12H, 5,15-(OC*H₃*)), 3.14 (br. s, 6H, 5,15-(*p*-OC*H₃*)).
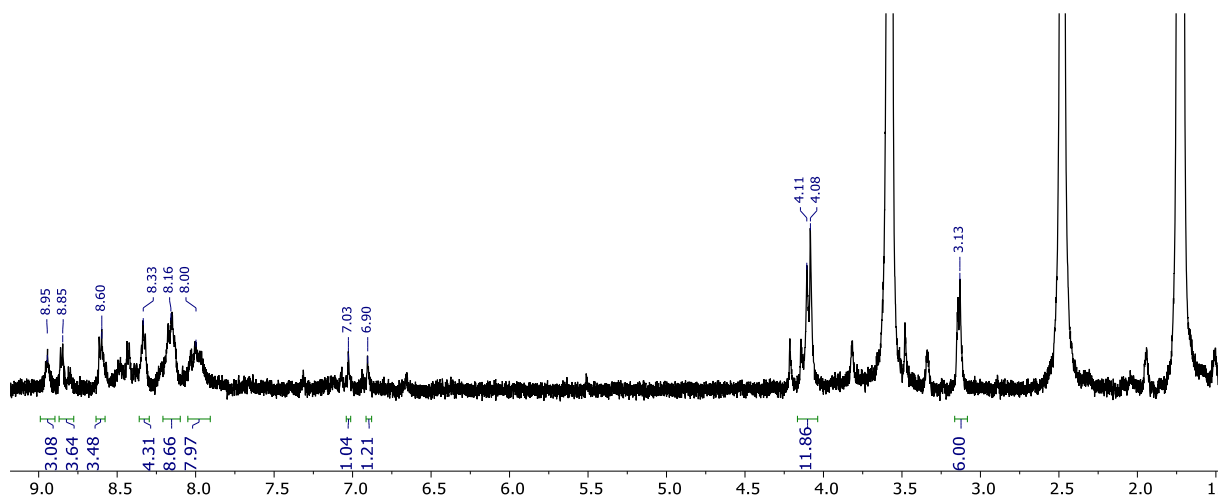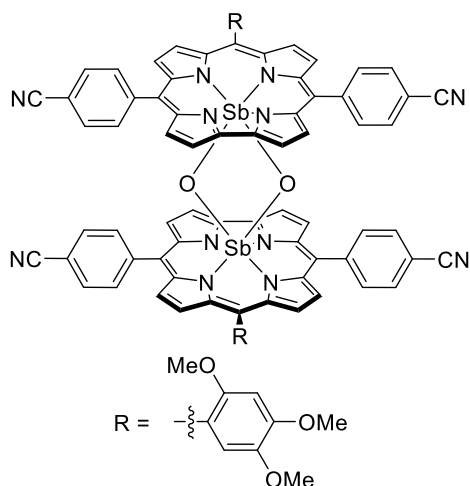

Figure S4. ^{1}H NMR of Di-μ-oxido-bis{5,15-di(4-cyanophenyl)-10-(2,4,5-trimethoxyphenyl)-corrolatoantimon(V)} in deuterated tetrahydrofuran (THF-d_8).

The NMR spectrum of the di-μ-oxido-complex reveals signals of different diastereomeric species due to restricted aryl group rotation. Therefore, we only used this compound as an intermediate in the synthesis of the dihalogenido complexes.

UV/vis (Dichloromethane): λ_{max} (ε [L·mol^{-1}·cm^{-1}]) = 298 (39800), 340 (22400), 416 (264800), 540 (12000), 577 (19600), 610 (45100) nm.

MS (ESI): m/z = 1600 ([M$_2$]), 800 ([M]$^+$), 784 ([M-O]$^+$).

CHN: Calc. for C$_{84}$H$_{54}$N$_{12}$O$_8$Sb$_2$ × 1.0 C$_6$H$_5$I (in %): C, 59.82; H, 3.29; N, 9.30. Found: C, 59.90; H, 3.30; N, 9.36.
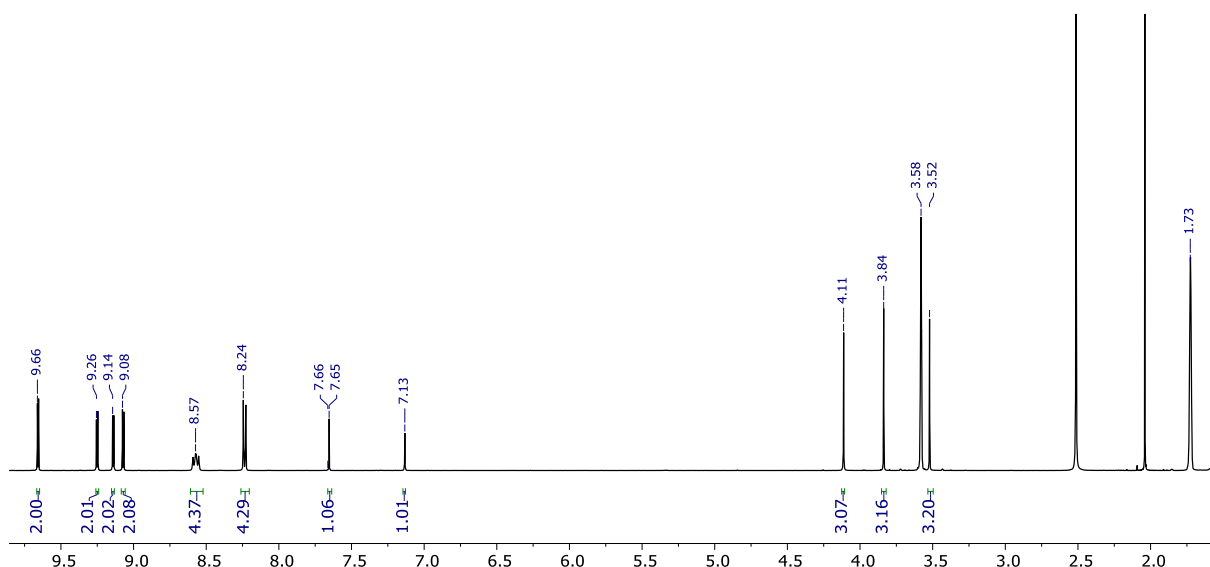
Figure S5. Structure of di-μ-oxido-bis{5,15-Bis(4-cyanophenyl)-10-(2,4,5-trimethoxyphenyl)corrolato-antimon(V)}.

Difluoro-5,15-di(4-cyanophenyl)-10-(2,4,5-trimethoxyphenyl)corrolatoantimon(V)

Di-μ-oxidoantimony(V)corrole (50 mg, 31 μmol) is treated with aqueous HF* (5 mL, 48%) in acetone (40 mL). The solution is stirred for 10 min at rt during which a greenish-blue colour change is observed. The crude mixture is extracted with dichloromethane (3 x 20 mL), washed with distilled water (2 x 30 mL) and dried over Na_2SO_4. After removal of the solvent and recrystallisation from dichloromethane/n-hexane, a blueish-green material (47 mg, 57 μmol, 91%) is obtained.

* Caution! Hydrofluoric acid is an extremely dangerous compound and precautions must be taken!

^{1}H NMR (500 MHz, THF-d_8) δ = 9.66 (d, J = 4.1 Hz, 2H, β-H), , 9.26 (d, J = 4.7 Hz, 2H, β-H), 9.14 (d, J = 4.1 Hz, 2H, β-H), 9.08 (d, J = 4.7 Hz, 2H, β-H), 8.60 – 8.54 (m, 4H, 5,15-(o-PhH)), 8.25 - 8.23 (m, 4H, 5,15-(m-PhH)), 7.66 (s, 1H, 10-(o-PhH)), 7.14 (s, 1H, 10-(m-PhH)), 4.12 (s, 3H, 10-(OCH_3)), 3.84 (s, 3H, 10-(OCH_3)), 3.53 (s, 3H, 10-(OCH_3)).
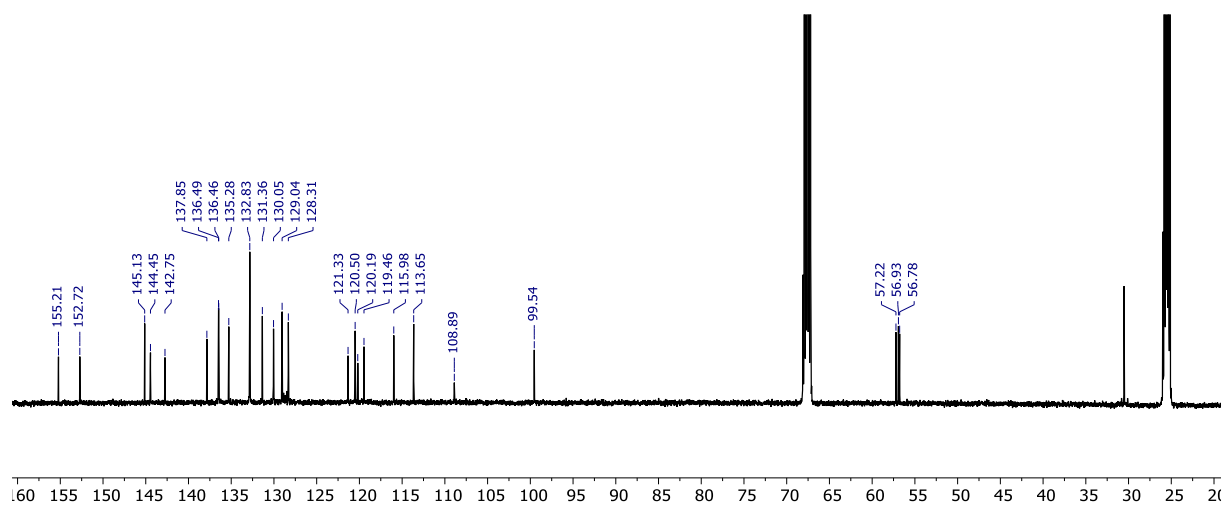

Figure S6. ^{1}H NMR of Difluoro-5,15-di(4-cyanophenyl)-10-(2,4,5-trimethoxyphenyl)-corrolatoantimon(V) in deuterated tetrahydrofuran (THF-d_8).

^{13}C NMR (126 MHz, THF-d_8) δ = 155.3 (s, 1C, 10-(PhCOCH$_3$)), 152.7 (s, 1C, 10-(PhCOCH$_3$)), 145.1 (s, 2C, 5,15-(CN-Ph), 144.5 (s, 1C, 10-(PhCOCH$_3$)), 142.8 (s, 2C, α-C), 137.9 (s, 2C, α-C), 136.5 (s, 4C, 5,15-(o-PhC), 135.3 (s, 2C, α-C), 132.8 (s, 4C, 5,15-(m-PhC)), 131.4 (s, 2C, α-C), 130.0 (s, 2C, β-C), 129.0 (s, 2C,
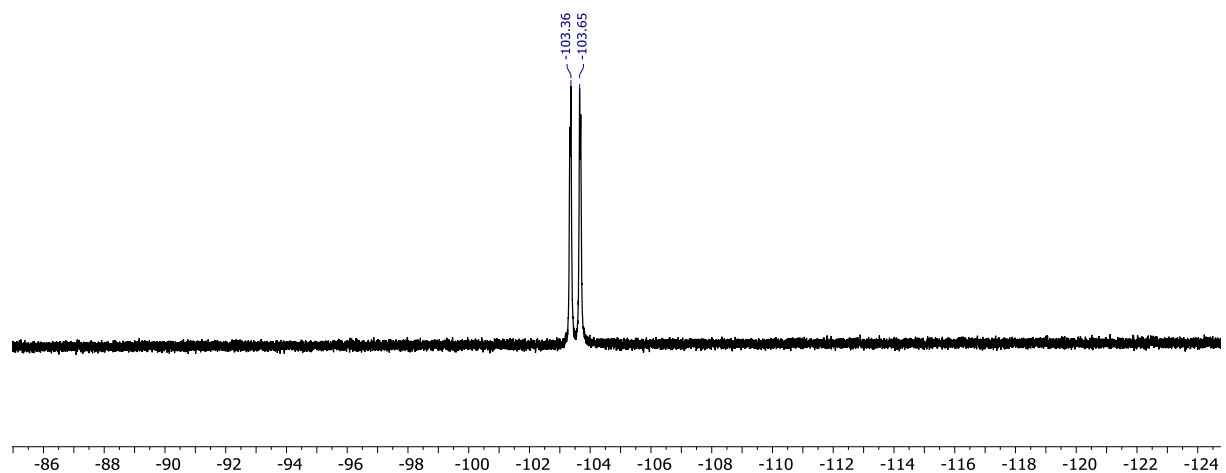
β-C), 128.3 (s, 2C, *β-C*), 121.3 (s, 1C, 10-(*o*-Ph*CH*)), 120.5 (s, 2C, *β-C*), 120.2(s, 1C, 10-(*ipso*-PhC)), 119.5 (2C, 5,15-(*ipso*-PhC)), 116.0 (s, 2C, *meso-C*), 113.7 (s, 2C, 5,15-(*p*-Ph*C*)), 108.9 (s, 1C, *meso-C*), 99.5 (s, 1C, 10-(*m*-Ph*CH*)), 57.2 (s, 1C, 10-(O*CH₃*)), 57.0 (s, 1C, 10-(O*CH₃*)), 56.8 (s, 1C, 10-(O*CH₃*)).

Figure S7. ^{13}C NMR of Difluoro-5,15-di(4-cyanophenyl)-10-(2,4,5-trimethoxyphenyl)-corrolatoantimon(V) in deuterated tetrahydrofuran (THF-d₈).

^{19}F NMR (377 MHz, THF-*d₈) δ* = -103.7 (d, 1F), -103.4 (d, 1F).

Figure S8. ^{19}F NMR of Difluoro-5,15-di(4-cyanophenyl)-10-(2,4,5-trimethoxyphenyl)-corrolatoantimon(V) in deuterated tetrahydrofuran (THF-d₈).

MS (ESI): m/z = 822 ([M]⁺), 803 ([M-F]⁺).

**UV/vis** (Dichloromethane): λ_max (ε [L·mol⁻¹·cm⁻¹]) = 341 (11400), 417 (156600), 534 (7600), 569 (12100), 607 (32400) nm.

CHN: Calc. for $C_{42}H_{27}F_2N_6O_3Sb$ x 1.1 CH_2Cl_2 (in %): C, 56.07; H, 3.20; N, 9.08. Found: C, 56.25; H, 3.66; N, 8.59.

Dichloro-5,15-di(4-cyanophenyl)-10-(2,4,5-trimethoxyphenyl)corrolatoantimon(V)

Di-μ-oxidoantimony(V)corrole (50 mg, 31 μmol) is treated with aqueous HCl (3 mL, 36%) in acetone (15 mL). The solution is stirred for 10 min at rt during which a greenish-blue colour change is observed. The crude mixture is extracted with dichloromethane (3 x 5 mL), washed with distilled water (2 x 5 mL) and dried over Na_2SO_4. After removal of the solvent and recrystallisation from dichloromethane/n-hexane, a blueish-green material (47 mg, 55 μmol, 88%) is obtained.

^{1}H NMR (500 MHz, THF-d_8) δ = 9.70 (d, J = 4.1 Hz, 2H, *β-H*), , 9.25 (d, J = 4.8 Hz, 2H, *β-H*), 9.13 (d, J = 4.1 Hz, 2H, *β-H*), 9.07 (d, J = 4.6 Hz, 2H, *β-H*), 8.63 (br. d, 2H, 5,15-(*o*-Ph*H*)), 8.54 (br. d, 2H, 5,15-(*o*-Ph*H*)), 8.30-8.25 (m, 4H, 5,15-(*m*-Ph*H*)), 7.64 (s, 1H, 10-(*o*-Ph*H*)), 7.15 (s, 1H, 10-(*m*-Ph*H*)), 4.12 (s, 3H, 10-(*p*-OC*H₃*)), 3.86 (s, 3H, 10-(OC*H₃*)), 3.45 (s, 3H, 10-(OC*H₃*)).
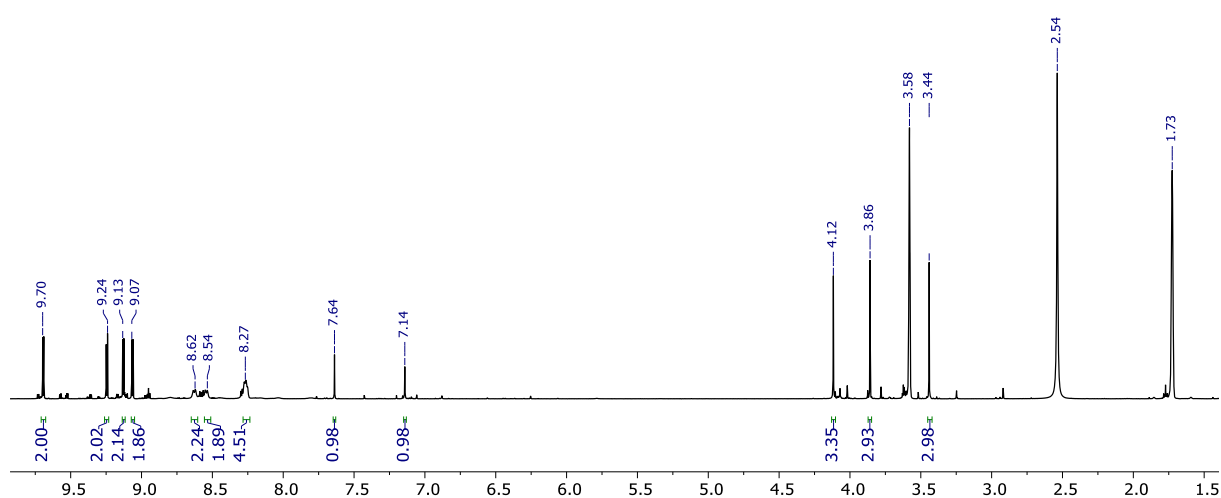
Figure S9. ^{1}H NMR of Dichloro-5,15-di(4-cyanophenyl)-10-(2,4,5-trimethoxyphenyl)-corrolatoantimon(V) in deuterated tetrahydrofuran (THF-d_8).

The NMR spectra reveal a second, unknown species, which may be attributed to a monochlorated species carrying a second ligand like thf, hydroxo or aqua. However, this species accounts for less than ten percent of the total composition, leading to no significant deviation in elemental analysis. Therefore, we still decided to analyse this compound with a bit of caution.

^{13}C NMR (126 MHz, THF-d_8) δ = 155.3 (s, 1C, 10-(Ph*C*OMe)), 152.7 (s, 1C, 10-(*p*-Ph*C*OMe)), 144.8 (s, 2C, 5,15-(*C*N-Ph), 144.5 (s, 1C, 10-(Ph*C*OMe)), 141.8 (s, 2C, *α-C*), 136.6 (s, 2C, *α-C*), 136.4 (s, 4C, 5,15-(*o*-Ph*C*), 135.7 (s, 2C, *α-C*), 132.8 (s, 4C, 5,15-(*m*-Ph*C*)), 130.9 (s, 2C, *α-C*), 129.5 (s, 2C, *β-C*), 129.1 (s, 2C, *β-C*), 127.8 (s, 2C, *β-C*), 121.1 (s, 1C, 10-(*o*-Ph*C*H)), 120.6 (s, 2C, *β-C*), 120.3 (s, 1C, 10-(*ipso*-Ph*C*)), 119.3 (s, 2C, 5,15-(*ipso*-Ph*C*)), 116.0 (s, 2C, *meso-C*), 113.7 (s, 2C, 5,15-(*p*-Ph*C*)), 109.1 (s, 1C, *meso-C*), 100.1 (s, 1C, 10-(*m*-Ph*C*H)), 57.4 (s, 1C, 10-(OC*H₃*)), 57.2 (s, 1C, 10-(OC*H₃*)), 56.6 (s, 1C, 10-(*p*-OC*H₃*)).
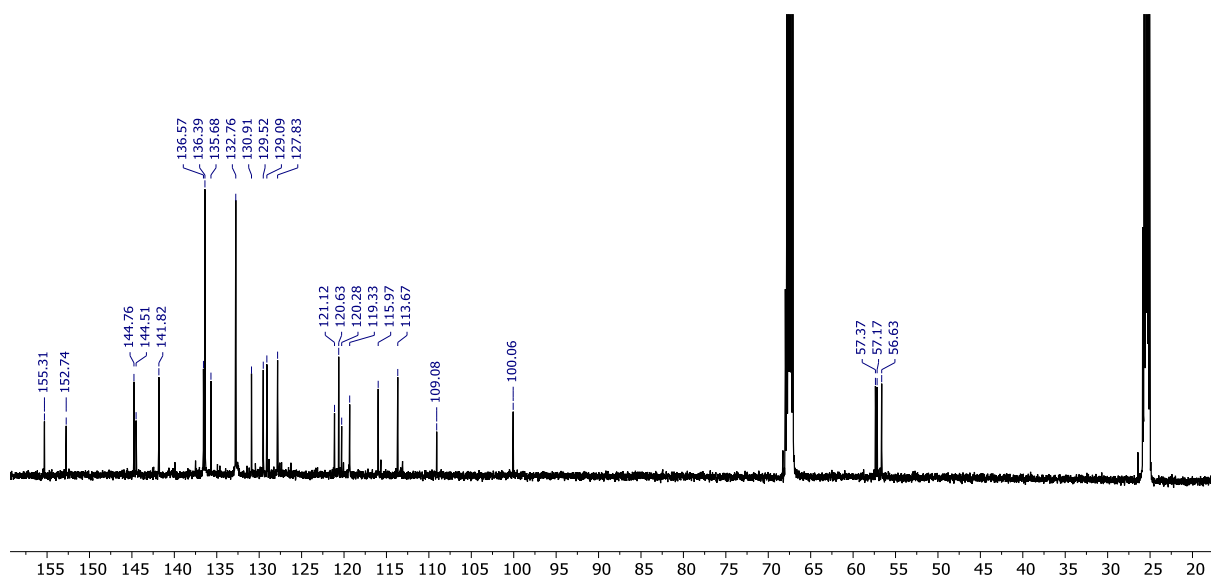
Figure S10. ^{13}C NMR of Dichloro-5,15-di(4-cyanophenyl)-10-(2,4,5-trimethoxyphenyl)-corrolatoantimon(V) in deuterated tetrahydrofuran (THF-d$_8$).

MS (ESI): m/z = 854 ([M]$^+$), 819 ([M-Cl]$^+$), 784 ([M-2Cl]$^+$).

UV/vis (Dichloromethane): λ_{max} (ϵ [L·mol^{-1}·cm^{-1}]) = 300 (22400), 424 (140700), 543 (7700), 576 (10600), 618 (27400) nm.

CHN: Cal. for C$_{42}$H$_{27}$Cl$_2$N$_6$O$_3$Sb (in %): C, 58.91; H, 3.18; N, 9.81. Found: C, 58.88; H, 3.33; N, 9.85.

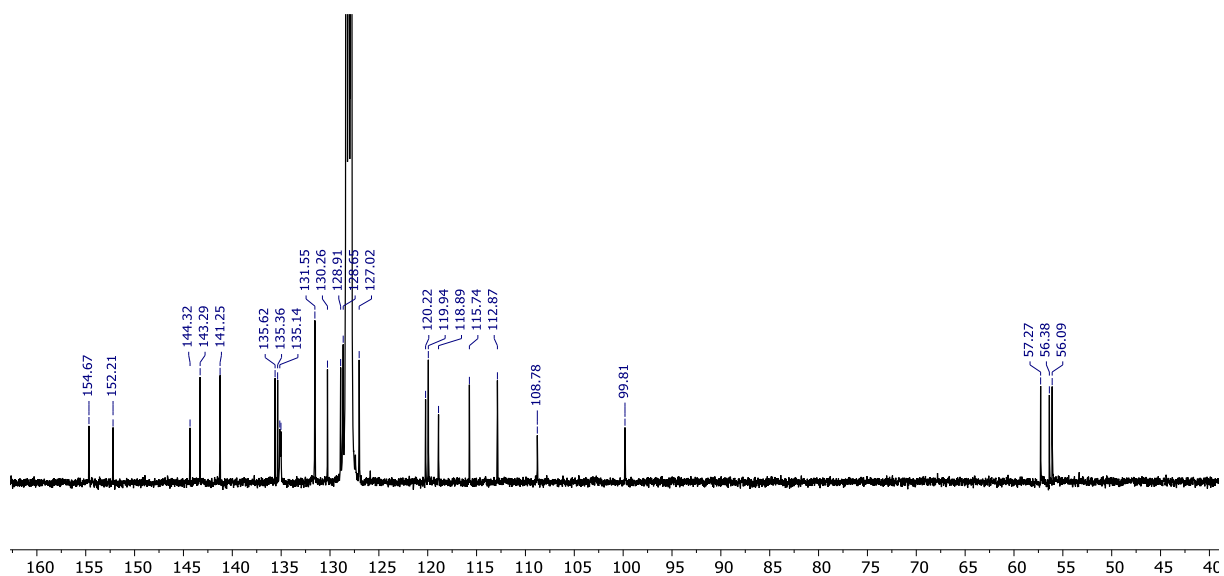**Dibromo-5,15-di(4-cyanophenyl)-10-(2,4,5-trimethoxyphenyl)corrolatoantimon(V)**

Antimony(III)corrole (50 mg, 66 µmol), dissolved in THF (40 mL), is treated dropwise with 6 mL of a bromine solution (0.1 mL Br_2 in 10 mL THF) until no further colour change to greenish-blue is observed. Stirring is continued for 10 min at RT until the reaction is terminated by removal of the solvent in vacuo. After recrystallisation from dichloromethane/n-hexane and drying in high vacuum, a blueish-green material (47mg, 50 µmol, 78%) is obtained.

¹H NMR (400 MHz, C_6D_6) δ = 9.11 (d, *J* = 4.1 Hz, 2H, *β-H*), , 9.07 (d, *J* = 4.8 Hz, 2H, *β-H*), 8.82 (d, *J* = 4.7 Hz, 2H, *β-H*), 8.60 (d, *J* = 4.1 Hz, 2H, *β-H*), 7.74 (s, 1H, 10-(*o*-Ph*H*)), 7.61 (d, *J* = 7.8 Hz, 2H, 5,15-(*o*-Ph*H*)), 7.53 (d, *J* = 7.8 Hz, 2H, 5,15-(*o*-Ph*H*)), 7.35 – 7.28 (m, 4H, 5,15-(*m*-Ph*H*)), 6.81 (s, 1H, 10-(*m*-Ph*H*)), 3.68 (s, 3H, 10-(OC*H*₃)), 3.40 (s, 3H, 10-(OC*H*₃)), 3.05 (s, 3H, 10-(OC*H*₃)).
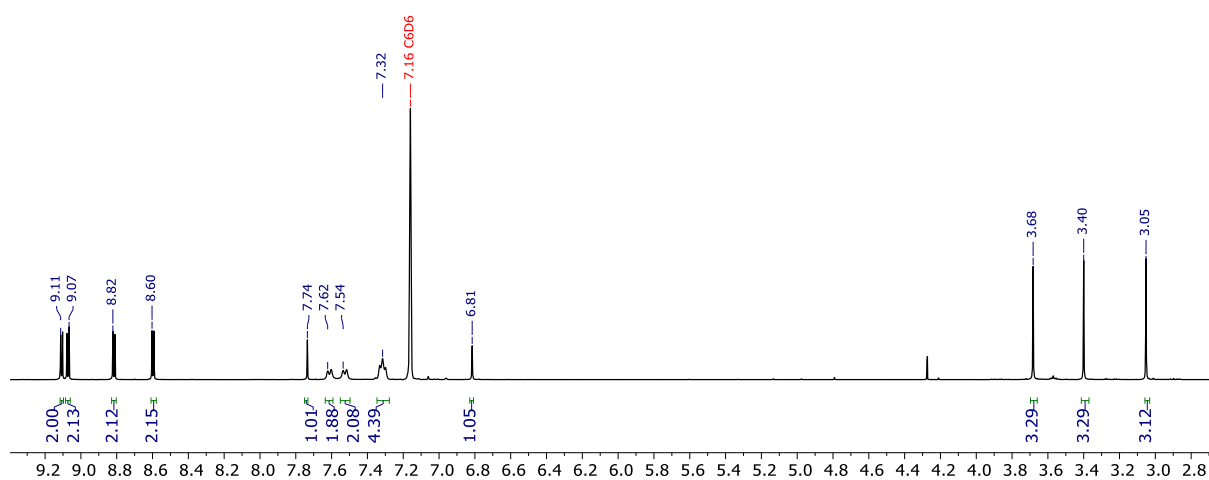
Figure S11. ¹H NMR of Dibromo-5,15-di(4-cyanophenyl)-10-(2,4,5-trimethoxyphenyl)-corrolatoantimon(V) in deuterated benzene (C_6D_6).

¹³C NMR (101 MHz, C_6D_6) δ = 154.7 (s, 1C, 10-(Ph*C*OMe)), 152.2 (s, 1C, 10-(Ph*C*OMe)), 144.3 (s, 1C, 10-(Ph*C*OMe)), 143.3 (s, 2C, 5,15-(*C*N-Ph), 141.3 (s, 2C, *α-C*), 135.6 (s, 2C, *α-C*), 135.4 (s, 2C, *α-C*), 135.1 (s, 2C, 5,15-(*o*-Ph*C*), 135.0 (s, 2C, 5,15-(*o*-Ph*C*), 131.6 (s, 4C, 5,15-(*m*-Ph*C*)), 130.3 (s, 2C, *α-C*), 128.9 (s, 2C, *β-C*), 128.7 (s, 2C, *β-C*), 127.0 (s, 2C, *β-C*), 120.2 (s, 1C, 10-(*o*-Ph*C*H)), 120.2(s, 1C, 10-(*ipso*-Ph*C*)), 119.9 (s, 2C, *β-C*), 118.9 (2C, 5,15-(*ipso*-Ph*C*)), 115.7 (s, 2C, *meso-C*), 112.9 (s, 2C, 5,15-(*p*-Ph*C*)), 108.8 (s, 1C, *meso-C*), 99.8 (s, 1C, 10-(*m*-Ph*C*H)), 57.3 (s, 1C, 10-(PhO*C*H₃)), 56.4 (s, 1C, 10-(PhO*C*H₃)), 56.1 (s, 1C, 10-(PhO*C*H₃)).

Figure S12. ^{13}C NMR of Dibromo-5,15-di(4-cyanophenyl)-10-(2,4,5-trimethoxyphenyl)-corrolatoantimon(V) in deuterated benzene (C_6D_6).

MS (ESI): m/z = 784 ([M-2Br]$^+$.

UV/vis (Dichloromethane): λ_{max} (ε [L·mol^{-1}·cm^{-1}]) = 305 (26200), 429 (133800), 545 (8200), 581 (11000), 623 (30800) nm.

CHN: Calc. for $C_{42}H_{27}Br_2N_6O_3Sb$ x 0.2 CH_2Cl_2 (in %): C, 52.67; H, 2.87; N, 8.73. Found: C, 53.37; H, 2.95; N, 8.39.

3 Emission Lifetime Measurements
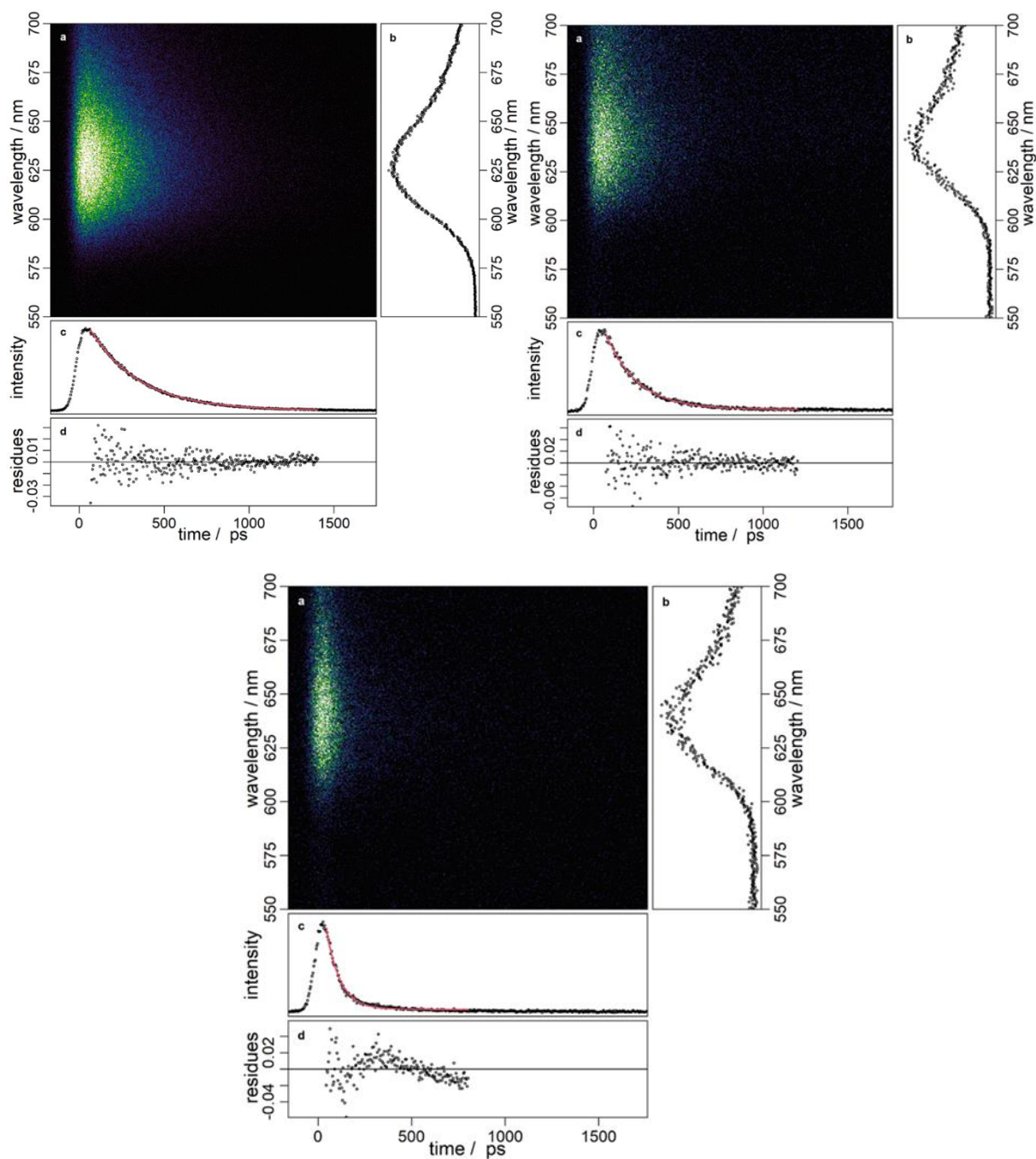
Figure S13. Streak camera measurement of **1** (top left), **2** (top right) and **3** (bottom) in inert dichloromethane; a) contour plot, b) emission spectrum, c) kinetic trace and d) residuals of kinetic fit. The emission lifetime is < 1 ns with 0.292 ns for **1**, 0.185 ns for **2** and 0.073 ns for **3**.

4 Singlet Oxygen Detection
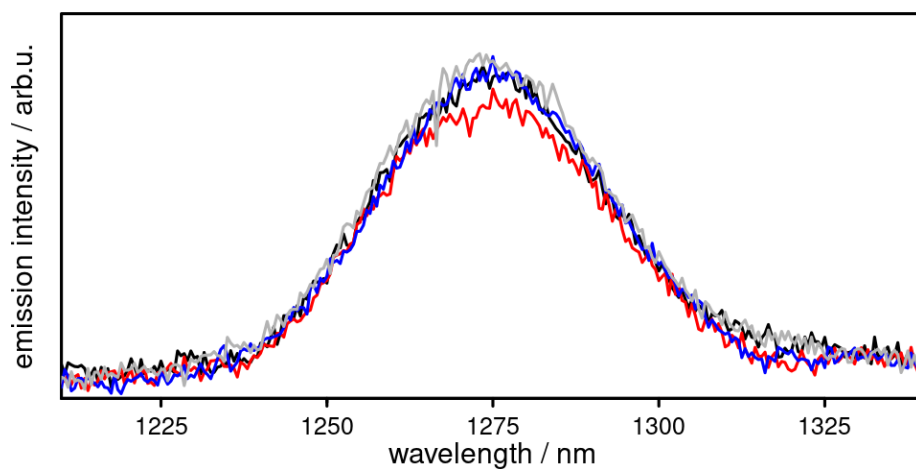
Figure S14. Singlet oxygen emission sensitised by **1** (black), **2** (red), **3** (blue) and **PN** (grey) in aerated dichloromethane. λ_{exc}=Soret band.
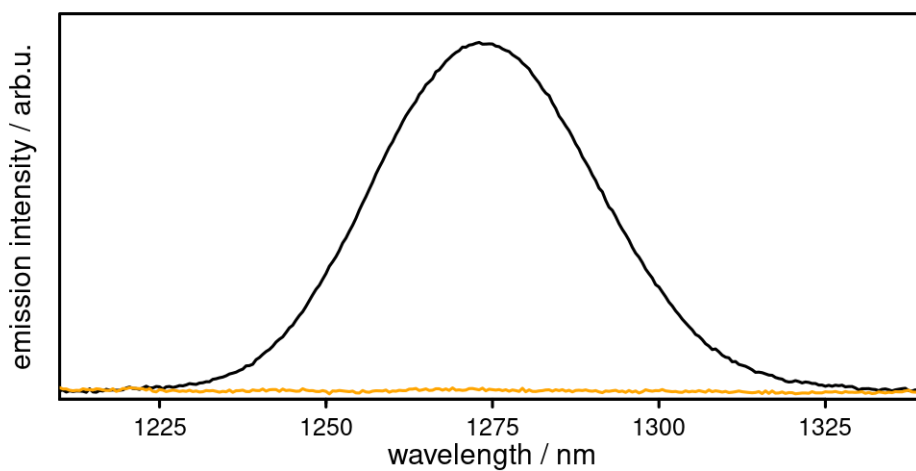
Figure S15. Singlet oxygen emission sensitised by **1** before (black) and after addition of 2,5-diphenylfuran (orange) in aerated, deuterated chloroform. As excitation wavelength the maximum of the Soret band were chosen (λ_{exc}=Soret band).

5 Transient Absorption Spectroscopy
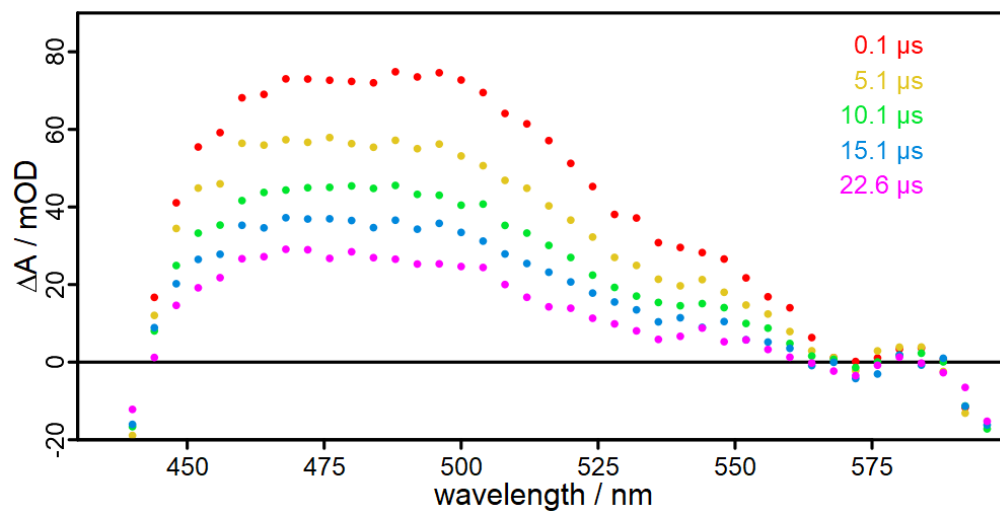
Figure S16. Transient absorption spectra of **1** in degassed dichloromethane at different delay times. The excitation wavelength λ_{exc} was chosen to be 355 nm.
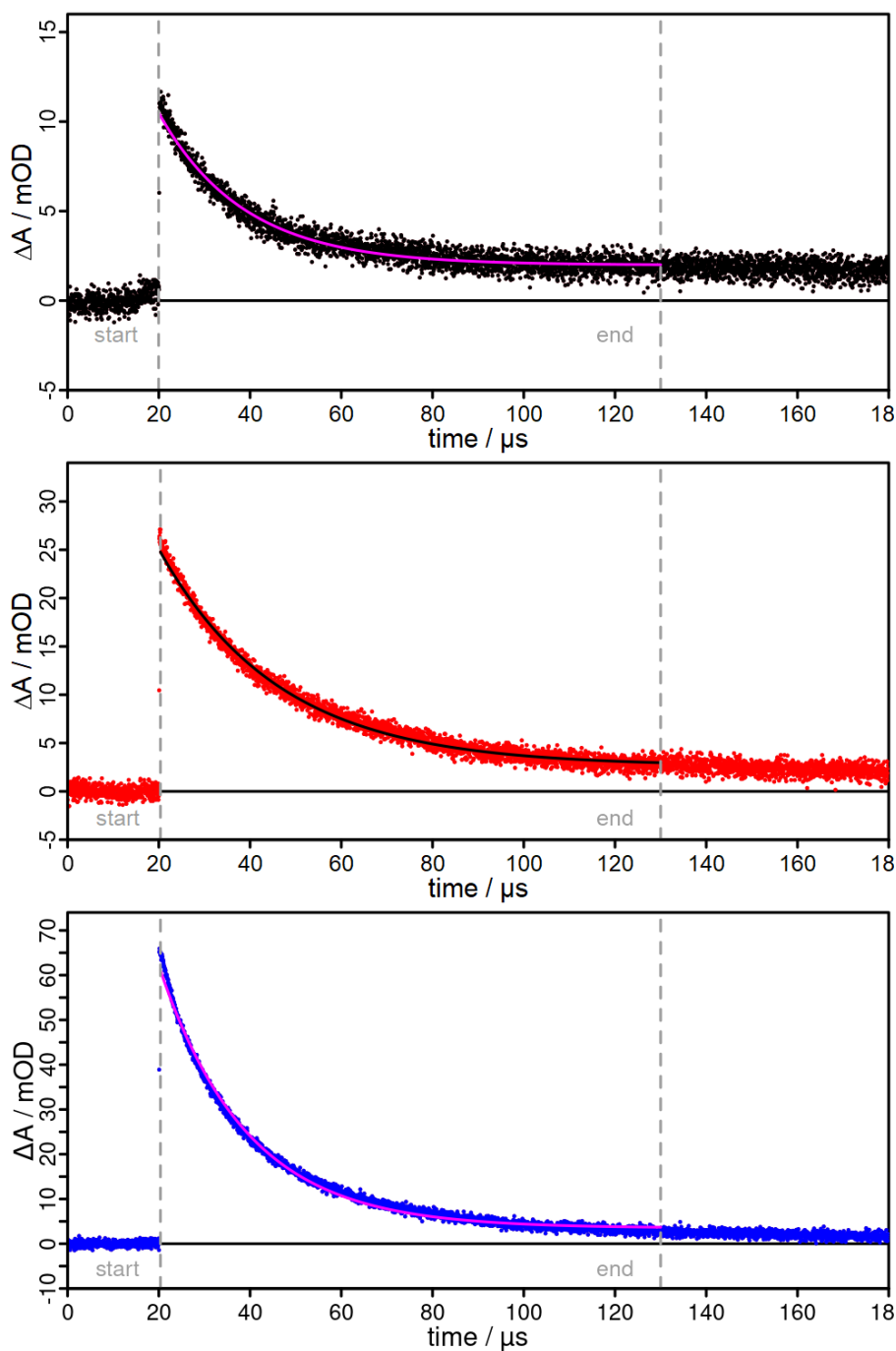
Figure S17. Kinetics of transient absorption measurements of **1** (black, top, fit at 490 nm), **2** (red, middle, fit at 500 nm) and **3** (blue, bottom, fit at 500 nm). The excitation wavelength λ_{exc} was chosen to be 355 nm and the exponential decay fit is highlighted in magenta (top and bottom) as well as black (middle). Decay times of 20.8 ± 0.20 µs for **1**, 28.8 ± 0.15 µs for **2** and 21.0 ± 0.01 µs for **3** were determined in degassed dichloromethane.

6 Photostability Measurements
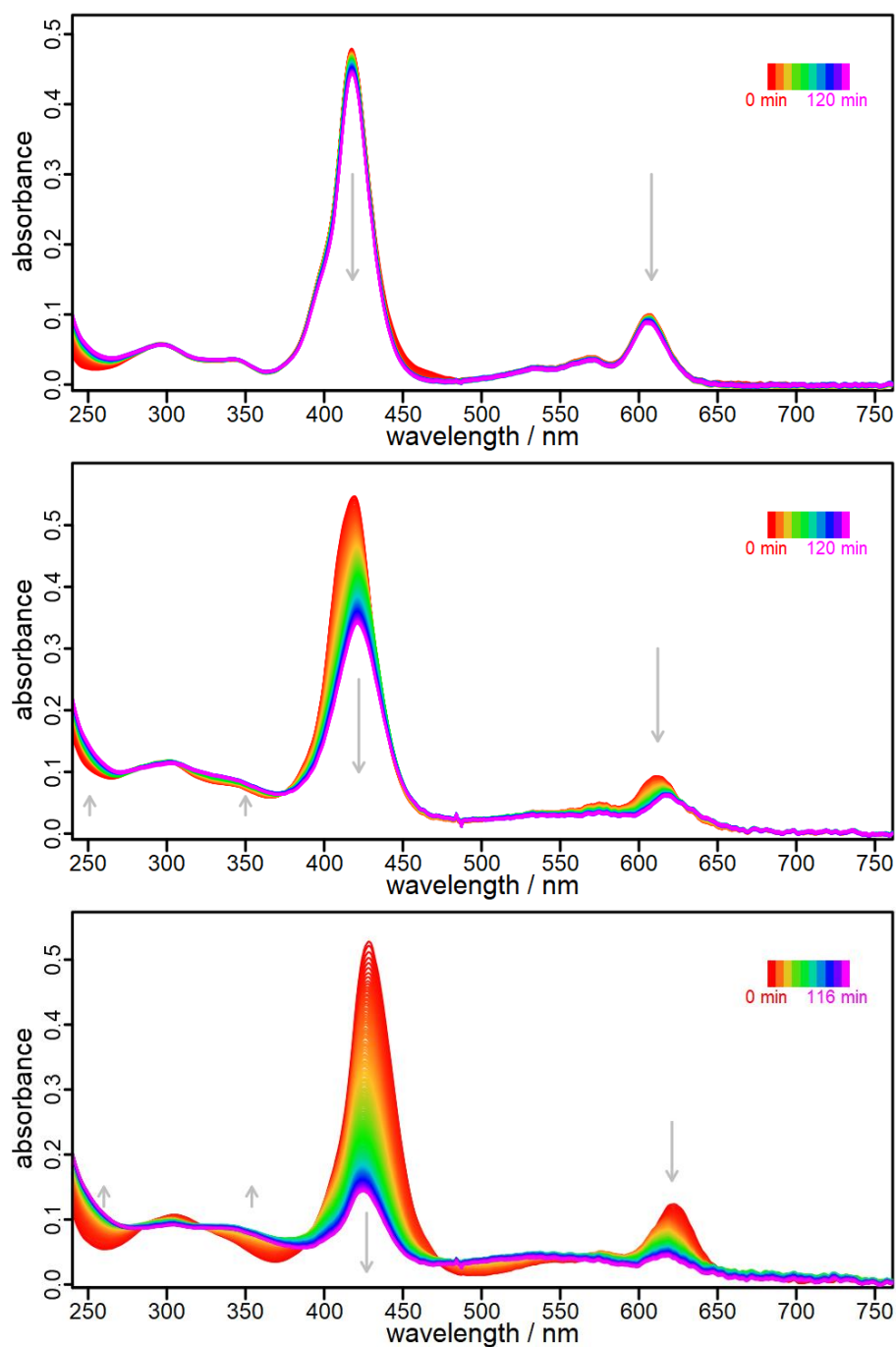
Figure S18. Photostability of **1** (top), **2** (bottom left) and **3** (bottom right) over the course of 2 h in aerated dichloromethane. Irradiated with a 150 W Xe-lamp and a long-pass filter > 400 nm was set in front of the sample.

7 Photocatalytic Oxidation of 2,5-Diphenylfuran *via* $^1O_2$
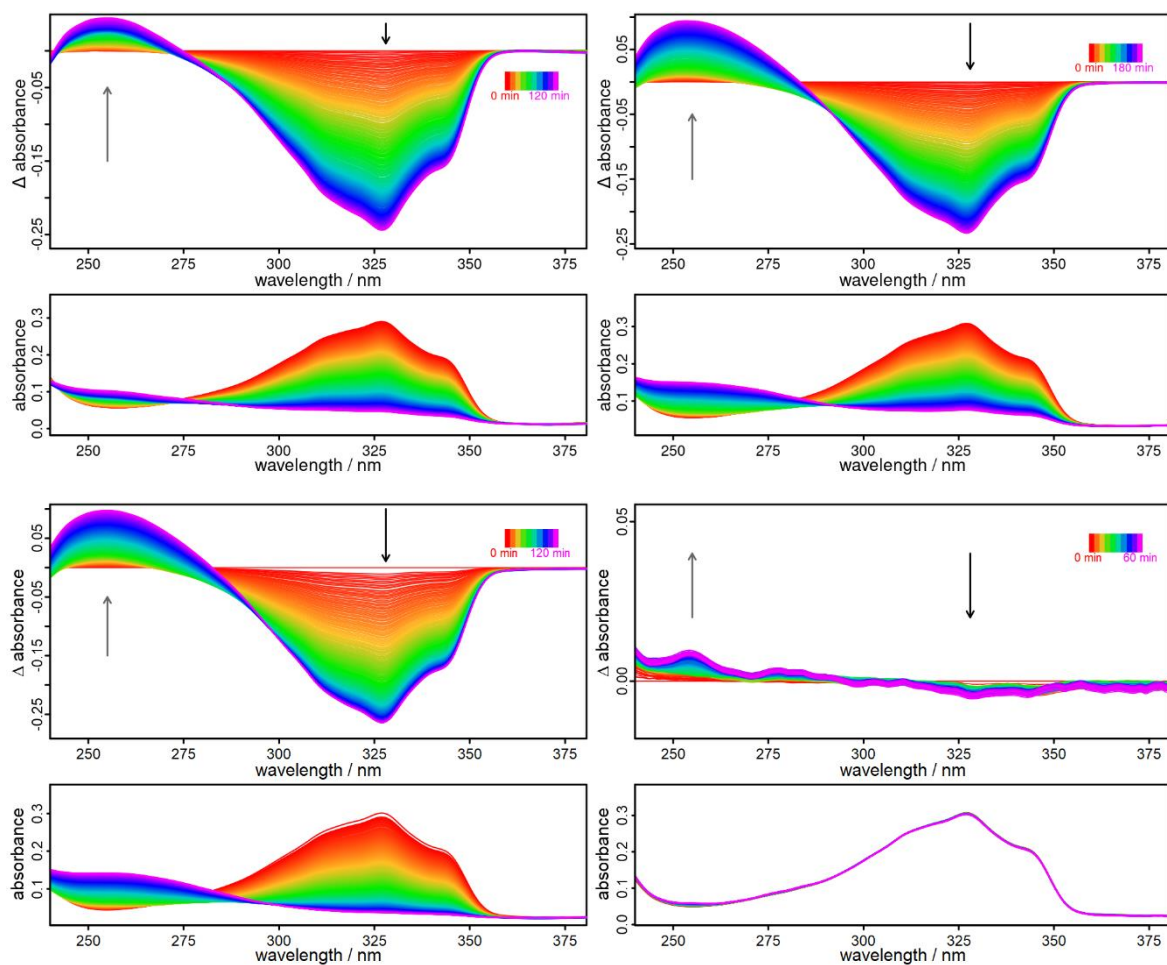
Figure S19. First hour of photocatalytic 2,5-diphenylfuran oxidation measurements of **1** (top left), **2** (top right), **3** (bottom left) and without PS (bottom right). *In situ* absorption spectra (top), differential absorption spectra (bottom) are shown. The absorption spectra show the absorbance values while the differential spectra show the difference compared to the first absorption spectrum (t=0).
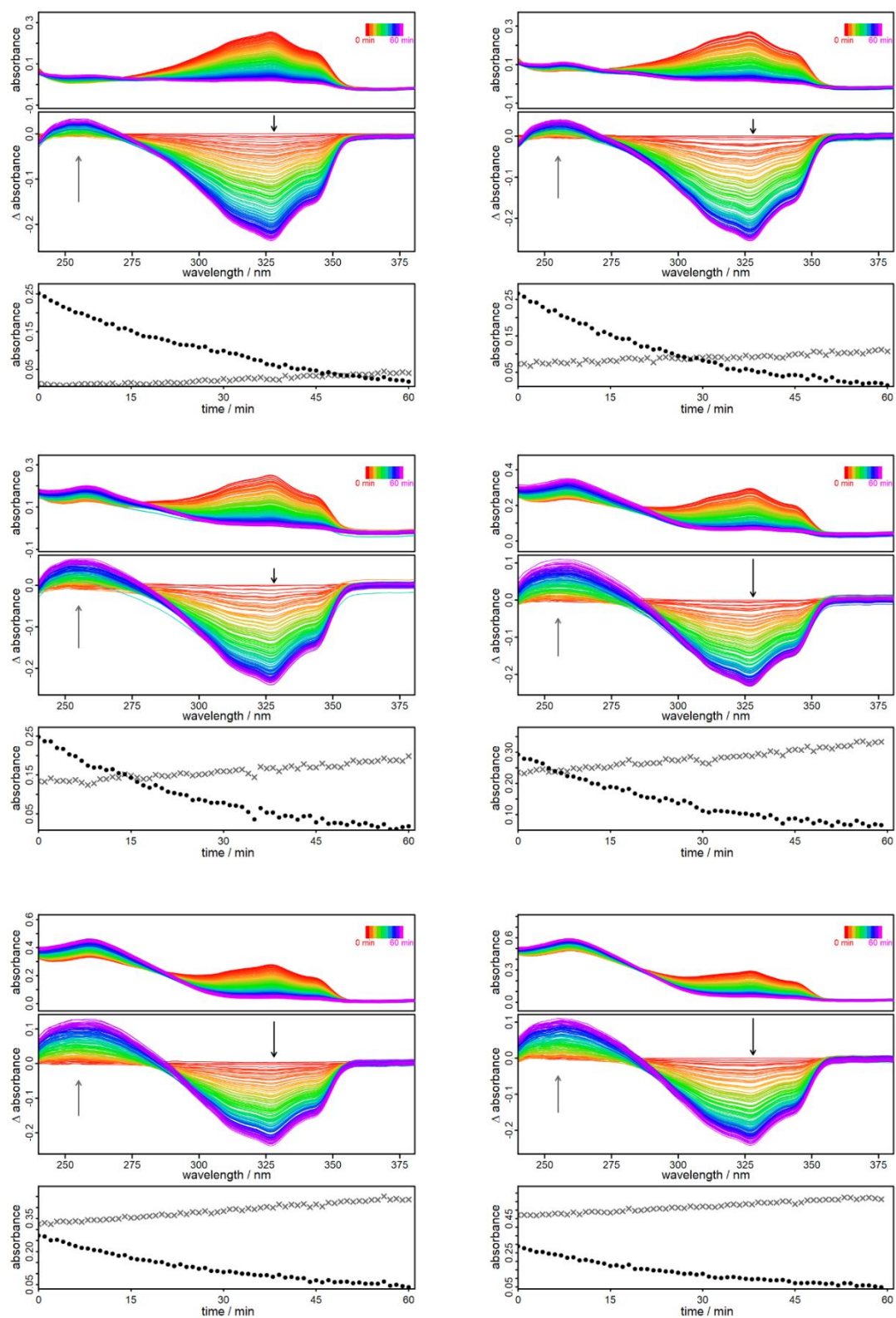
Figure S20. *In situ* absorption spectra (top), differential absorption spectra (middle) and time dependent absorbance values (bottom) for 2,5-diphenylfuran depletion (λ=328 nm, black dots) and diketone generation (λ=255 nm, grey crosses) using **1** are shown. First (top left), second (top right), third (middle left), fourth (middle right), fifth (bottom left) and sixth cycle (bottom right) are presented respectively.

The slight increase of the diketone signal upon addition of 2,5-diphenylfuran is due to the small absorbance of the latter at 255 nm (see Fig. S20, blank measurement). However, compared to the product, its absorptivity is lower and thus an increase in signal intensity upon conversion is observable. In the following, initial conversion rates are calculated using only the first hour of experiment, neglecting any error occurring from this phenomenon.
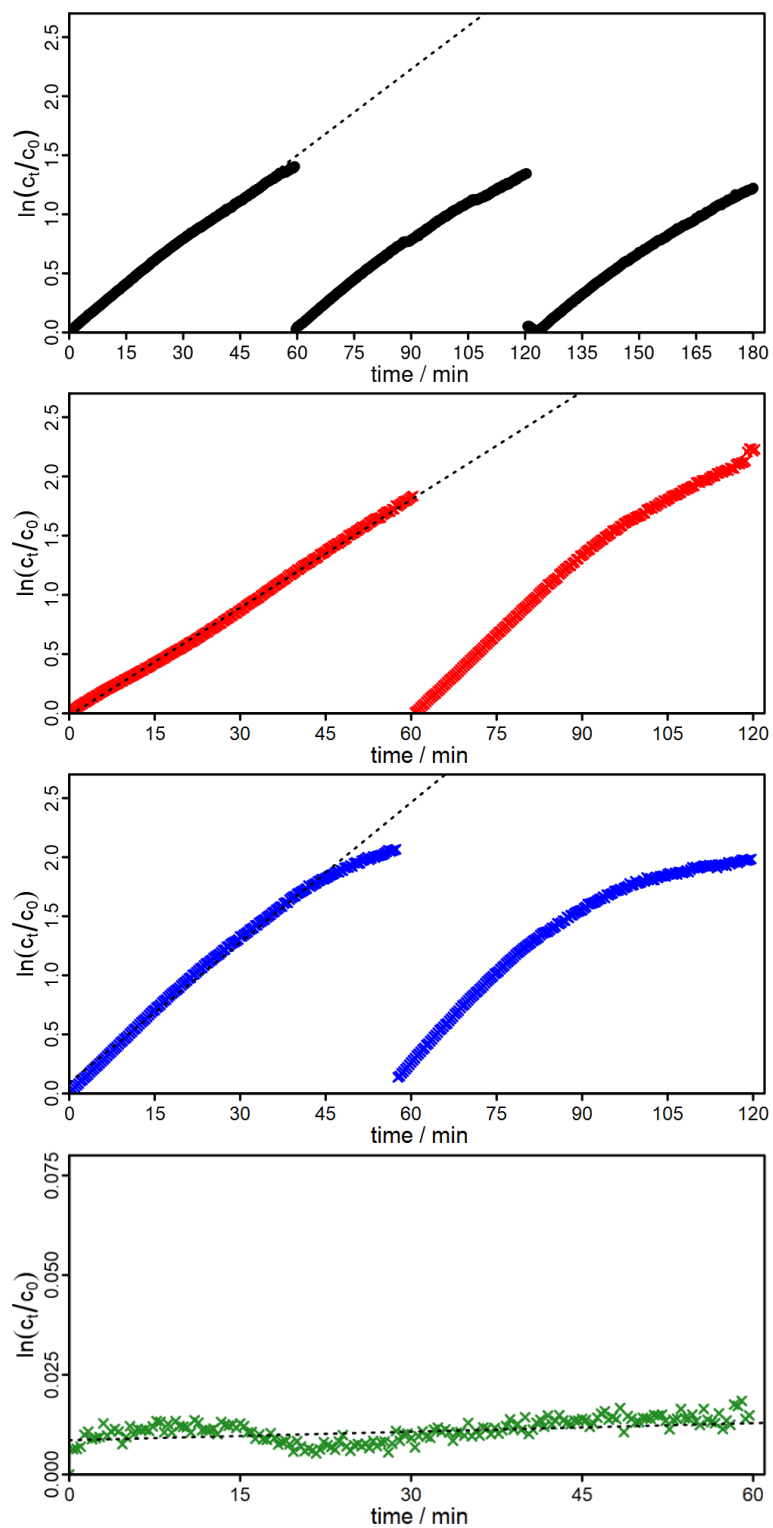
The photocatalytic 2,5-diphenylfuran conversion was observed over time by *in situ* absorption spectroscopy. To gain further knowledge about the kinetics, the absorbance at 355 nm (assigned to 2,5-diphenylfuran) is fitted using a pseudo-first order kinetic fit. The initial concentration (c_0) and the concentration after time t (c_t) of 2,5-diphenylfuran are described using the absorbance/extinction A and the molar attenuation coefficient ε (eq. S3 and S4 respectively). Since a division of c_t by c_0 is done to calculate the initial rate constant of 2,5-diphenylfuran conversion k_{DPF} (eq. S5), the knowledge about the absorbance A (at a specific wavelength λ) at the beginning (A_0) and after time t (A_t) is sufficient. These values are derived from the *in situ* absorption measurements directly.

$$\frac{A_{\lambda,t}}{\varepsilon_{DPF} \cdot d} = \frac{\log\left(\frac{I_0}{I_t}\right)}{\varepsilon_{DPF} \cdot d} = c_t \qquad\qquad \text{eq. S3}$$

$$\frac{A_{\lambda,0}}{\varepsilon_{DPF} \cdot d} = \frac{\log\left(\frac{I_0}{I}\right)}{\varepsilon_{DPF} \cdot d} = c_0 \qquad\qquad \text{eq. S4}$$

$$k_{DPF} = \frac{\ln\left(\frac{c_t}{c_0}\right)}{t} = \ln\frac{\left(\frac{A_{\lambda,t} \cdot \varepsilon_{DPF} \cdot d}{\varepsilon_{DPF} \cdot d \cdot A_{\lambda,0}}\right)}{t} = \frac{\ln\left(\frac{A_{\lambda,t}}{A_{\lambda,0}}\right)}{t} \qquad\qquad \text{eq. S5}$$

Figure S21. Logarithmic conversion *vs.* time plots. 2,5-diphenylfuran rates k_{DPF} are determined by applying a pseudo-first order kinetic fit (linear fit) and deriving its slope. The k_{DPF} was calculated to be 0.0243 min^{-1} for **1** (black), 0.0304 min^{-1} for **2** (red), 0.0305 min^{-1} for **3** (blue) and 7.1*10^{-5} min^{-1} for the blank measurement (green).

8 Computational Data – DFT and TDDFT
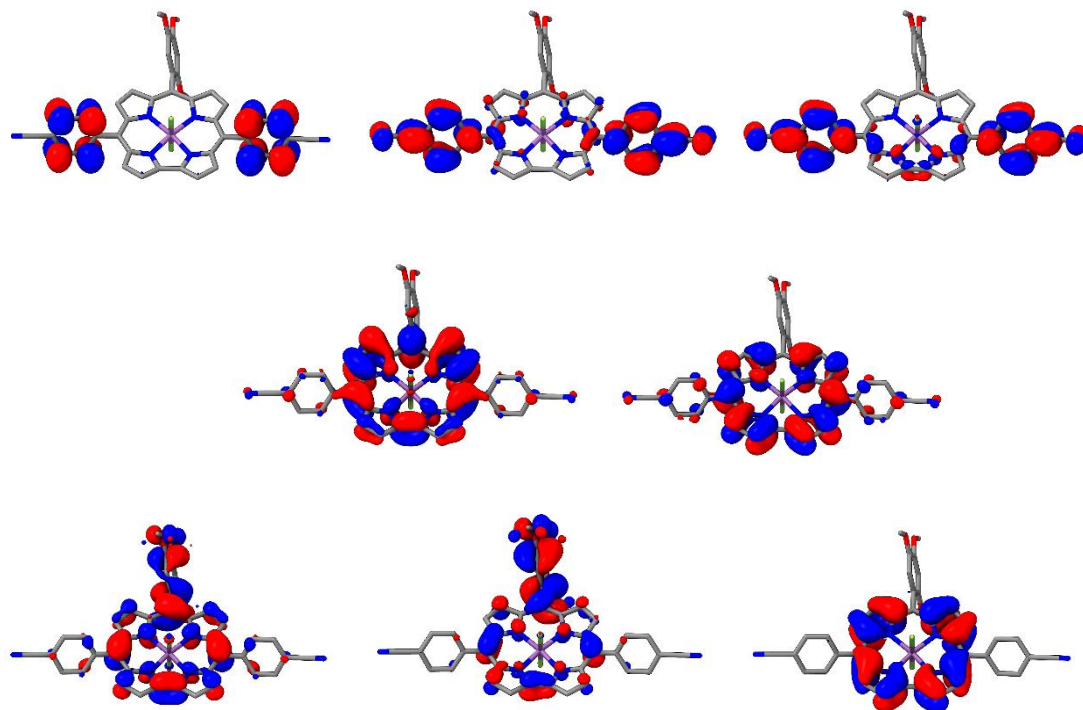
Figure S22 Calculated molecular orbitals of **1** in dichloromethane. Shown are in the top row: LUMO+4, LUMO+3, LUMO+2; in the middle row: LUMO+1 and LUMO; and in the bottom row: HOMO, HOMO-1, HOMO-2.
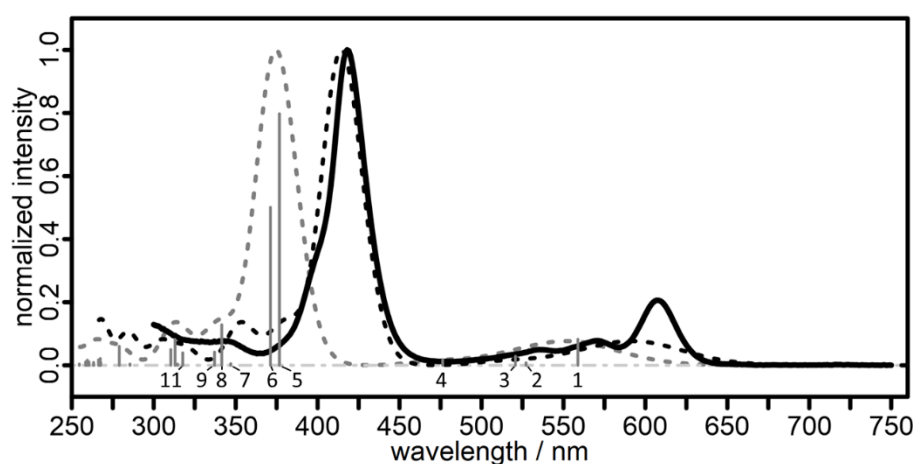
Figure S23. Calculated M06/def2-TZVPP (without shift: gray dotted; with a 40 nm shift: black dotted) *vs.* experimental (black solid) absorption spectrum of **1** in dichloromethane. Every bar shows an excitation wavelength and absolute oscillator strength (scaled down by 1/3) of a single excitation $S_x \leftarrow S_0$.

$S_1 \leftarrow S_0$

$S_2 \leftarrow S_0$

$S_3 \leftarrow S_0$

$S_4 \leftarrow S_0$

$S_5 \leftarrow S_0$

$S_6 \leftarrow S_0$

$S_7 \leftarrow S_0$

$S_8 \leftarrow S_0$

$S_9 \leftarrow S_0$

$S_{11} \leftarrow S_0$
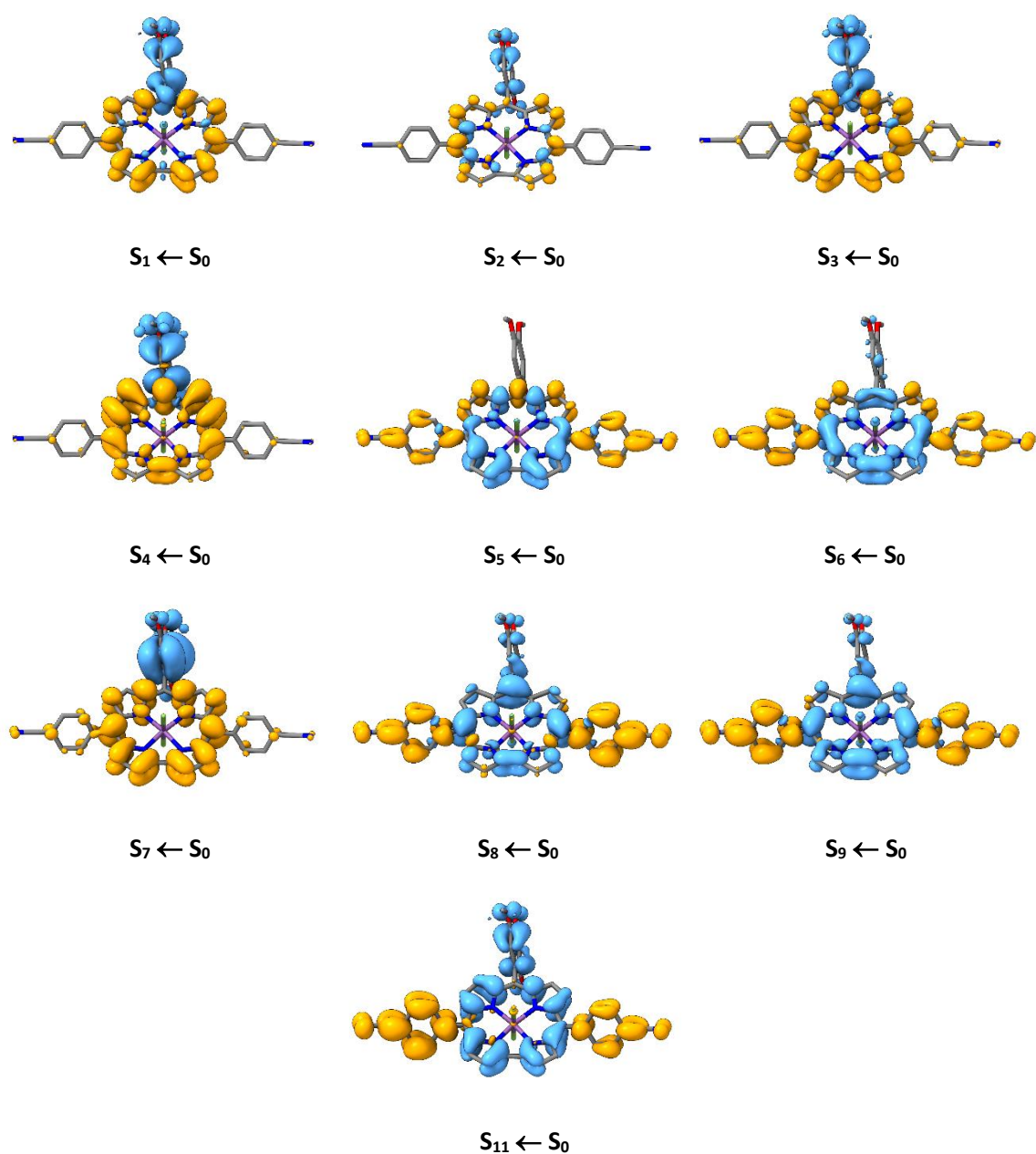
Figure S24. Electronic difference density plots of **1**. Each plot shows the electron density migrating from blue to orange during the excitation $S_x \leftarrow S_0$. The transition $S_{10} \leftarrow S_0$ is not shown due to having an oscillator strength < 0.01.

Table S1. Excitation energies in cm^{-1} and nm, oscillator strengths f_{osc} and corresponding transitions of **1** obtained from TDDFT with M06/def2-TZVPP calculated with implicit dichloromethane. Excitations with an oscillator strength > 0.01 and corresponding orbital contributions ≥ 0.1 (|coeff.|^2 ≥ 0.1) are shown.

| State	Exc. energy		f_{osc}	Dominant contribution			Transition
#	cm^{-1}	nm		OC	occ. orb.	virt. orb.	
1	17895.2	558.8	0.247	0.137	HOMO-2	LUMO+1	$\pi_C \rightarrow \pi_C{}^*$
				0.835	HOMO	LUMO	$\pi_C, \pi_{PhOMe} \rightarrow \pi_C{}^*$
2	18967.8	527.2	0.024	0.367	HOMO-2	LUMO	$\pi_C \rightarrow \pi_C{}^*$
				0.194	HOMO-1	LUMO	$\pi_C, \pi_{PhOMe} \rightarrow \pi_C{}^*$
				0.378	HOMO	LUMO+1	$\pi_C, \pi_{PhOMe} \rightarrow \pi_C{}^*$
3	19204.3	520.7	0.087	0.135	HOMO-2	LUMO	$\pi_C \rightarrow \pi_C{}^*$
				0.681	HOMO-1	LUMO	$\pi_C, \pi_{PhOMe} \rightarrow \pi_C{}^*$
4	20997.3	476.3	0.054	0.679	HOMO-1	LUMO+1	$\pi_C, \pi_{PhOMe} \rightarrow \pi_C{}^*$
				0.238	HOMO	LUMO+1	$\pi_C, \pi_{PhOMe} \rightarrow \pi_C{}^*$
5	26545.0	376.7	2.392	0.584	HOMO-2	LUMO+1	$\pi_C \rightarrow \pi_C{}^*$
				0.108	HOMO	LUMO	$\pi_C, \pi_{PhOMe} \rightarrow \pi_C{}^*$
				0.108	HOMO	LUMO+3	$\pi_C, \pi_{PhOMe} \rightarrow \pi_{PhCN}{}^*$
6	26941.0	371.2	1.503	0.303	HOMO-2	LUMO	$\pi_C \rightarrow \pi_C{}^*$
				0.217	HOMO-1	LUMO+1	$\pi_C, \pi_{PhOMe} \rightarrow \pi_C{}^*$
				0.241	HOMO	LUMO+1	$\pi_C, \pi_{PhOMe} \rightarrow \pi_C{}^*$
				0.108	HOMO	LUMO+2	$\pi_C, \pi_{PhOMe} \rightarrow \pi_{PhCN}{}^*$
7	28820.7	347.0	0.016	0.968	HOMO-3	LUMO	$\pi_{PhOMe} \rightarrow \pi_C{}^*$
8	29282.6	341.5	0.385	0.743	HOMO	LUMO+2	$\pi_C, \pi_{PhOMe} \rightarrow \pi_{PhCN}{}^*$
9	29664.3	337.1	0.126	0.712	HOMO	LUMO+3	$\pi_C, \pi_{PhOMe} \rightarrow \pi_{PhCN}{}^*$
11	31479.3	317.7	0.119	0.530	HOMO-2	LUMO+2	$\pi_C \rightarrow \pi_{PhCN}{}^*$
				0.233	HOMO-1	LUMO+2	$\pi_C, \pi_{PhOMe} \rightarrow \pi_{PhCN}{}^*$

C = Corrole ring, PhOMe = Trimethoxyphenyl ring, PhCN = Cyanophenyl rings
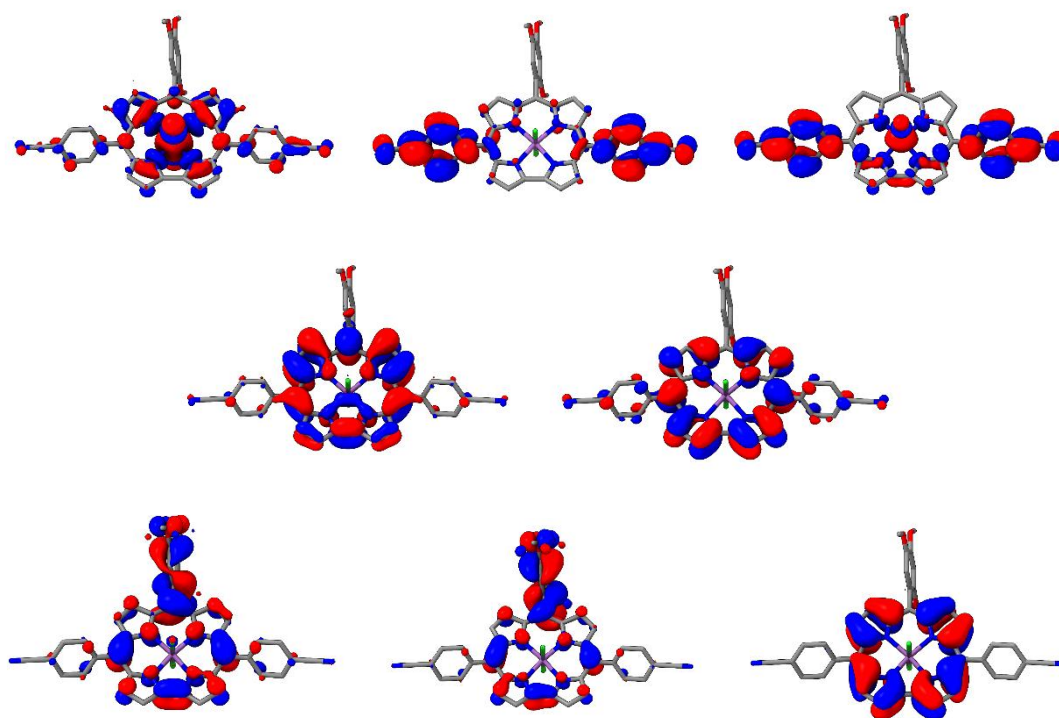
Figure S25. Calculated molecular orbitals of **2** in dichloromethane. Shown are in the top row: LUMO+4, LUMO+3, LUMO+2; in the middle row: LUMO+1 and LUMO; and in the bottom row: HOMO, HOMO-1, HOMO-2.
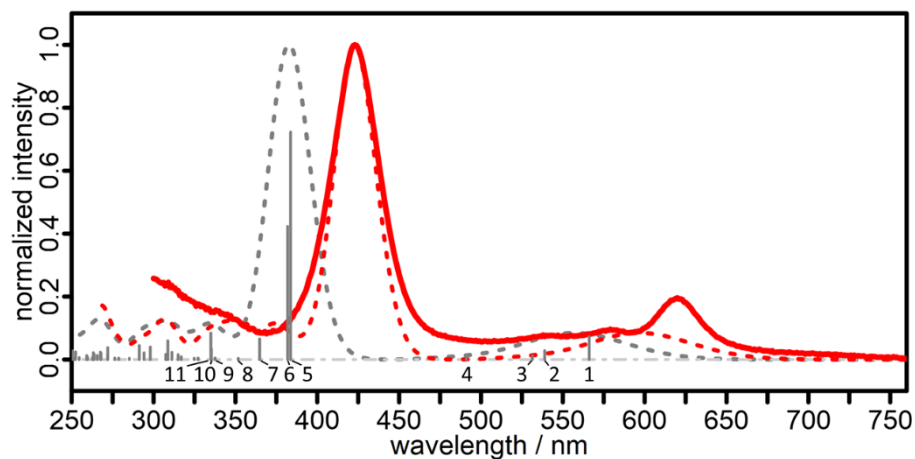
Figure S26. Calculated M06/def2-TZVPP (without shift: gray dotted; with a 40 nm shift: red dotted) *vs.* experimental (red solid) absorption spectrum of **2** in dichloromethane. Every bar shows an excitation wavelength and absolute oscillator strength (scaled down by 1/3) of a single excitation $S_x \leftarrow S_0$.

$S_1 \leftarrow S_0$ $S_2 \leftarrow S_0$ $S_3 \leftarrow S_0$

$S_4 \leftarrow S_0$ $S_5 \leftarrow S_0$ $S_6 \leftarrow S_0$

$S_7 \leftarrow S_0$ $S_8 \leftarrow S_0$ $S_9 \leftarrow S_0$

$S_{10} \leftarrow S_0$ $S_{11} \leftarrow S_0$
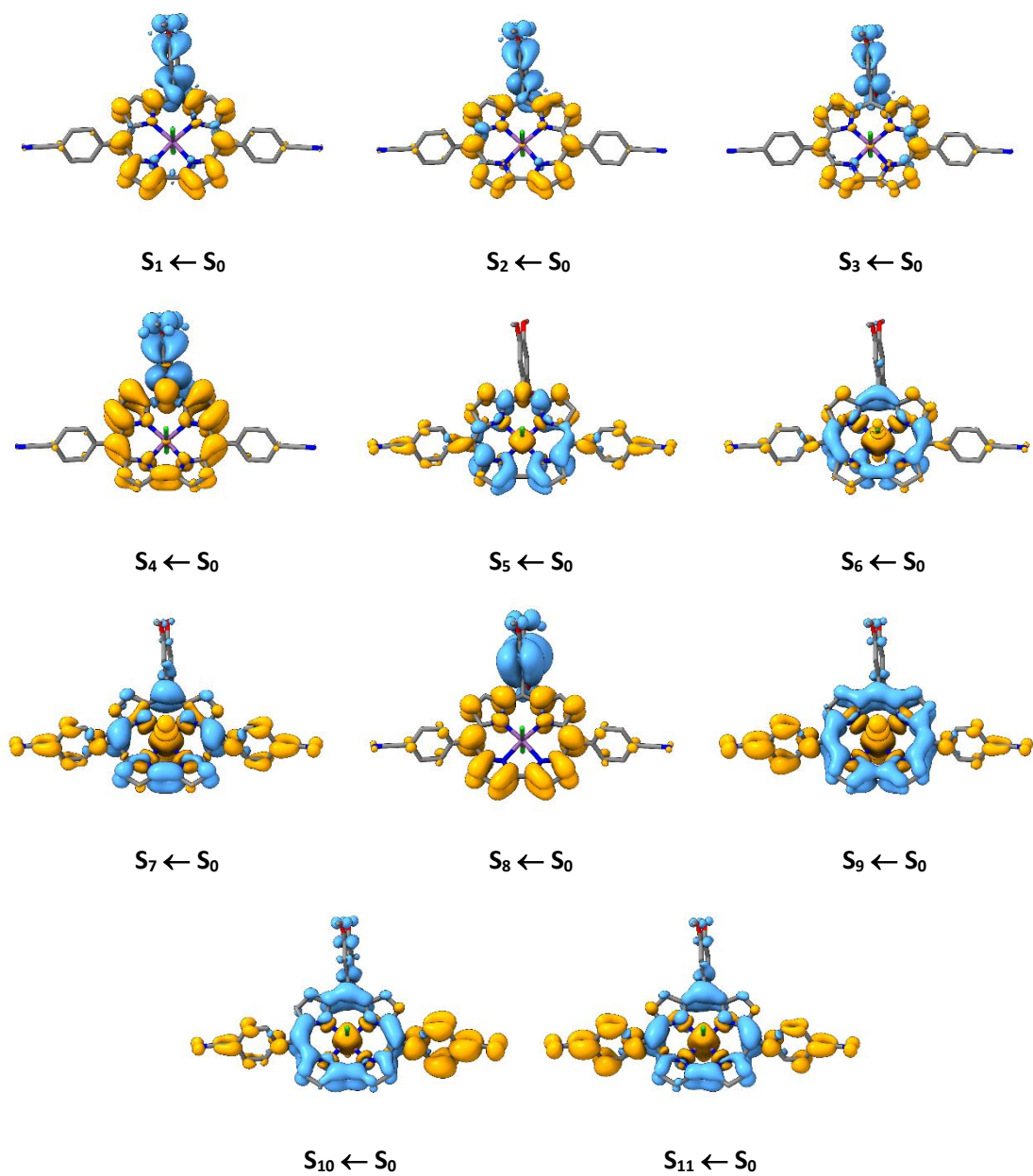
Figure S27. Electronic difference density plots of **2**. Each plot shows the electron density migrating from blue to orange during the excitation $S_x \leftarrow S_0$.

Table S2. Excitation energies in cm^{-1} and nm, oscillator strengths f_{osc} and corresponding transitions of **2** obtained from TDDFT with M06/def2-TZVPP calculated with implicit dichloromethane. Excitations with an oscillator strength > 0.01 and corresponding orbital contributions ≥ 0.1 ($|$coeff.$|^2$ ≥ 0.1) are shown.

| State	Exc. energy		f_{osc}	Dominant contribution			Transition
#	cm^{-1}	nm		OC	occ. orb.	virt. orb.	
1	17665.3	566.1	0.219	0.130	HOMO-2	LUMO+1	$\pi_C \rightarrow \pi_C{}^*$
				0.843	HOMO	LUMO	$\pi_{C,}\pi_{PhOMe} \rightarrow \pi_C{}^*$
2	18555.9	538.9	0.085	0.116	HOMO-2	LUMO	$\pi_C \rightarrow \pi_C{}^*$
				0.603	HOMO-1	LUMO	$\pi_{C,}\pi_{PhOMe} \rightarrow \pi_C{}^*$
				0.180	HOMO	LUMO+1	$\pi_{C,}\pi_{PhOMe} \rightarrow \pi_C{}^*$
3	18819.1	531.4	0.037	0.349	HOMO-2	LUMO	$\pi_C \rightarrow \pi_C{}^*$
				0.265	HOMO-1	LUMO	$\pi_{C,}\pi_{PhOMe} \rightarrow \pi_C{}^*$
				0.286	HOMO	LUMO+1	$\pi_{C,}\pi_{PhOMe} \rightarrow \pi_C{}^*$
4	20361.8	491.1	0.029	0.670	HOMO-1	LUMO+1	$\pi_{C,}\pi_{PhOMe} \rightarrow \pi_C{}^*$
				0.256	HOMO	LUMO+1	$\pi_{C,}\pi_{PhOMe} \rightarrow \pi_C{}^*$
5	26059.6	383.7	2.169	0.594	HOMO-2	LUMO+1	$\pi_C \rightarrow \pi_C{}^*$
				0.105	HOMO	LUMO	$\pi_{C,}\pi_{PhOMe} \rightarrow \pi_C{}^*$
6	26183.6	381.9	1.269	0.349	HOMO-2	LUMO	$\pi_C \rightarrow \pi_C{}^*$
				0.175	HOMO-1	LUMO+1	$\pi_{C,}\pi_{PhOMe} \rightarrow \pi_C{}^*$
				0.185	HOMO	LUMO+1	$\pi_{C,}\pi_{PhOMe} \rightarrow \pi_C{}^*$
				0.119	HOMO	LUMO+4	$\pi_{C,}\pi_{PhOMe} \rightarrow \sigma_{Sb-X}{}^*$
7	27408.8	364.8	0.196	0.141	HOMO-1	LUMO+2	$\pi_{C,}\pi_{PhOMe} \rightarrow \sigma_{Sb-X}{}^*, \pi_{PhCN}{}^*$
				0.484	HOMO	LUMO+2	$\pi_{C,}\pi_{PhOMe} \rightarrow \sigma_{Sb-X}{}^*, \pi_{PhCN}{}^*$
				0.196	HOMO	LUMO+4	$\pi_{C,}\pi_{PhOMe} \rightarrow \sigma_{Sb-X}{}^*$
8	28429.7	351.7	0.012	0.989	HOMO-3	LUMO	$\pi_{PhOMe} \rightarrow \pi_C{}^*$
9	29624.6	337.6	0.015	0.201	HOMO-2	LUMO+2	$\pi_C \rightarrow \sigma_{Sb-X}{}^*, \pi_{PhCN}{}^*$
				0.305	HOMO-2	LUMO+4	$\pi_C \rightarrow \sigma_{Sb-X}{}^*$
				0.340	HOMO	LUMO+3	$\pi_{C,}\pi_{PhOMe} \rightarrow \pi_{PhCN}{}^*$
10	29823.6	335.3	0.099	0.208	HOMO-2	LUMO+2	$\pi_C \rightarrow \sigma_{Sb-X}{}^*, \pi_{PhCN}{}^*$
				0.341	HOMO	LUMO+3	$\pi_{C,}\pi_{PhOMe} \rightarrow \pi_{PhCN}{}^*$
11	29852.3	335.0	0.252	0.214	HOMO	LUMO+2	$\pi_{C,}\pi_{PhOMe} \rightarrow \sigma_{Sb-X}{}^*, \pi_{PhCN}{}^*$
				0.348	HOMO	LUMO+4	$\pi_{C,}\pi_{PhOMe} \rightarrow \sigma_{Sb-X}{}^*$

C = Corrole ring, PhOMe = Trimethoxyphenyl ring, PhCN = Cyanophenyl rings, Sb-X = Antimony-halide bonds
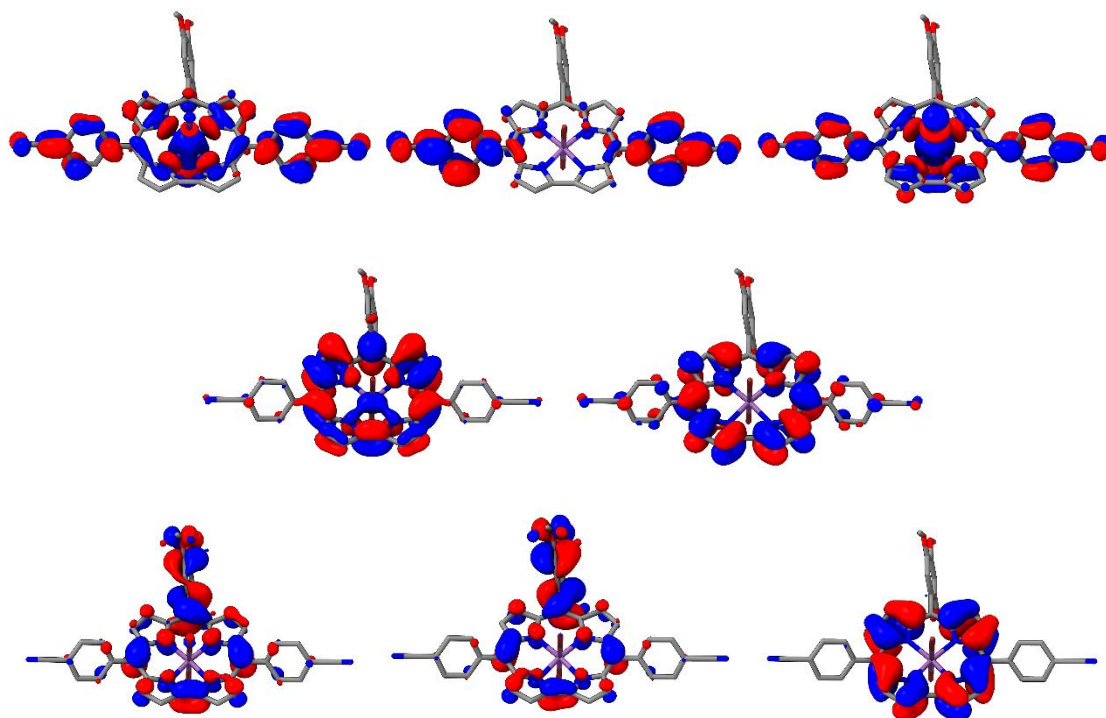
Figure S28. Calculated molecular orbitals of **3** in dichloromethane. Shown are in the top row: LUMO+4, LUMO+3, LUMO+2; in the middle row: LUMO+1 and LUMO; and in the bottom row: HOMO, HOMO-1, HOMO-2.
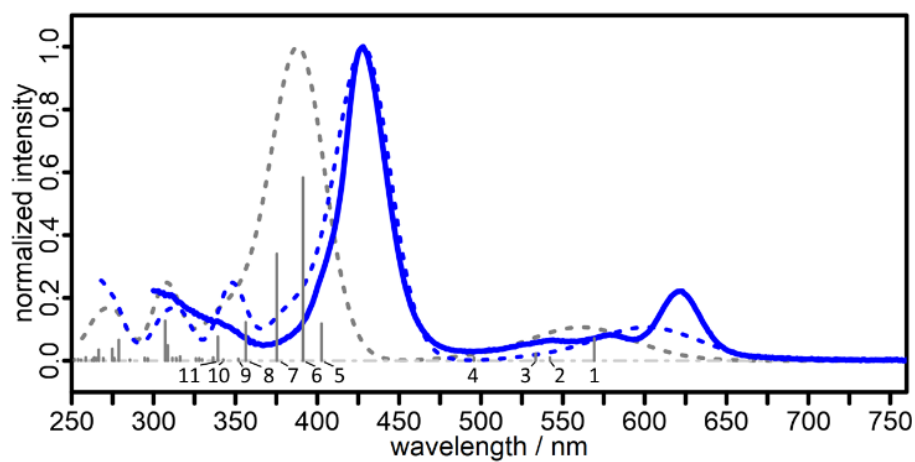
Figure S29. Calculated M06/def2-TZVPP (without shift: gray dotted; with a 40 nm shift: blue dotted) *vs*. experimental (blue) absorption spectrum of **3** in dichloromethane. Every bar shows an excitation wavelength and absolute oscillator strength (scaled down by 1/3) of a single excitation $S_x \leftarrow S_0$.

$S_1 \leftarrow S_0$ $S_2 \leftarrow S_0$ $S_3 \leftarrow S_0$

$S_4 \leftarrow S_0$ $S_5 \leftarrow S_0$ $S_6 \leftarrow S_0$

$S_7 \leftarrow S_0$ $S_8 \leftarrow S_0$ $S_9 \leftarrow S_0$

$S_{10} \leftarrow S_0$ $S_{11} \leftarrow S_0$
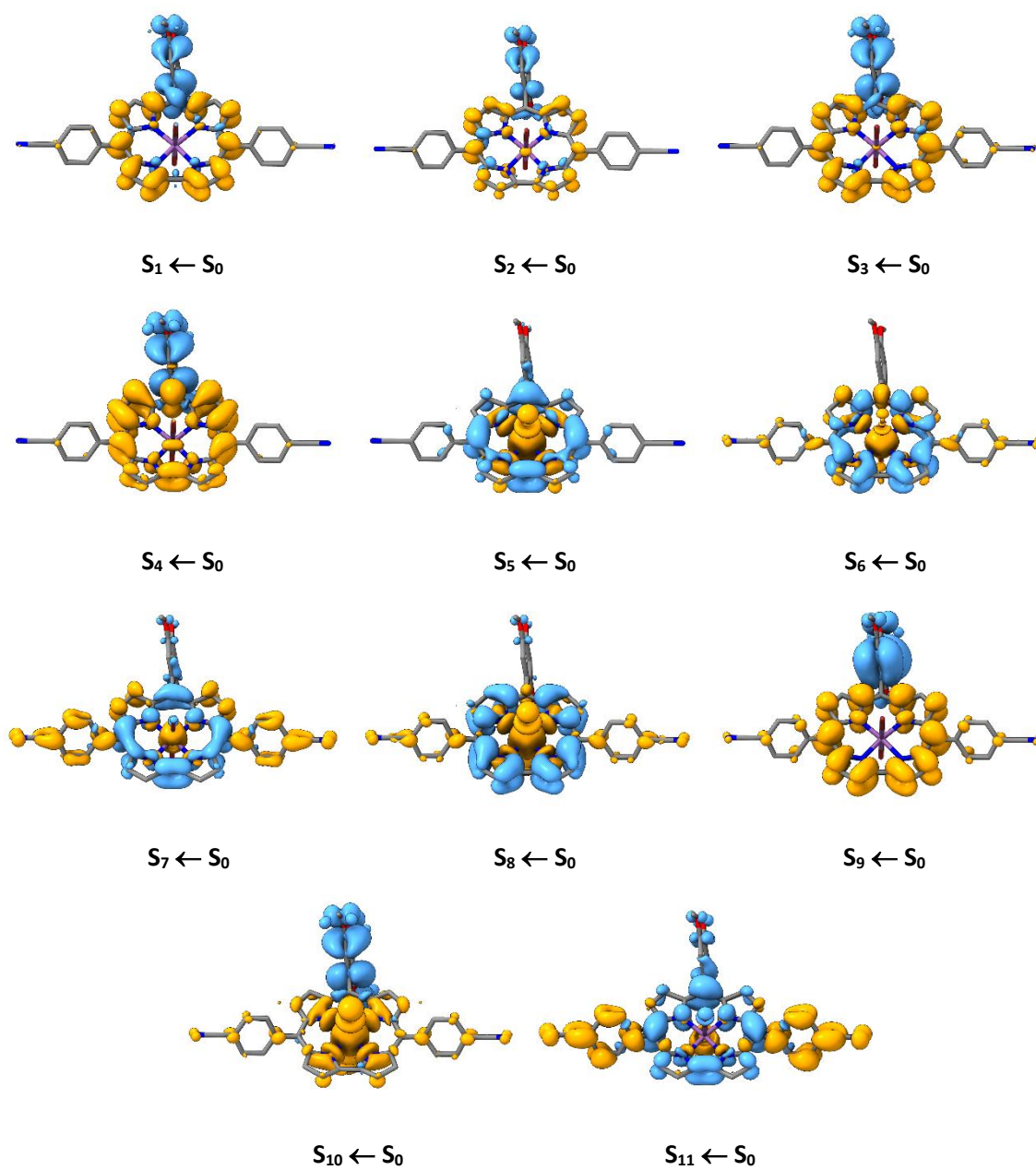
Figure S30. Electronic difference density plots of **3**. Each plot shows the electron density migrating from blue to orange during the excitation $S_x \leftarrow S_0$.

Table S3. Excitation energies in cm^{-1} and nm, oscillator strengths f_{osc} and corresponding transitions of **3** obtained from TDDFT with M06/def2-TZVPP simulated in dichloromethane. Excitations with an oscillator strength > 0.01 and corresponding orbital contributions ≥ 0.1 (|coeff.|^2 ≥ 0.1) are shown.

State	Exc. energy		f_{osc}	Dominant contribution			Transition
#	cm^{-1}	nm		OC	occ. orb.	virt. orb.	
1	17569.7	569.2	0.214	0.141	HOMO-2	LUMO+1	$\pi_C \rightarrow \pi_C$*
				0.837	HOMO	LUMO	$\pi_C, \pi_{PhOMe} \rightarrow \pi_C$*
2	18445.4	542.1	0.031	0.259	HOMO-2	LUMO	$\pi_C \rightarrow \pi_C$*
				0.278	HOMO-1	LUMO	$\pi_C, \pi_{PhOMe} \rightarrow \pi_C$*
				0.383	HOMO	LUMO+1	$\pi_C, \pi_{PhOMe} \rightarrow \pi_C$*
3	18747.3	533.4	0.068	0.166	HOMO-2	LUMO	$\pi_C \rightarrow \pi_C$*
				0.586	HOMO-1	LUMO	$\pi_C, \pi_{PhOMe} \rightarrow \pi_C$*
				0.125	HOMO	LUMO+1	$\pi_C, \pi_{PhOMe} \rightarrow \pi_C$*
4	20175.1	495.7	0.030	0.676	HOMO-1	LUMO+1	$\pi_C, \pi_{PhOMe} \rightarrow \pi_C$*
				0.238	HOMO	LUMO+1	$\pi_C, \pi_{PhOMe} \rightarrow \pi_C$*
5	24837.6	402.6	0.354	0.188	HOMO-2	LUMO	$\pi_C \rightarrow \pi_C$*
				0.111	HOMO-1	LUMO+2	$\pi_C, \pi_{PhOMe} \rightarrow \sigma_{Sb-X}$*, π_{PhCN}*
				0.317	HOMO	LUMO+2	$\pi_C, \pi_{PhOMe} \rightarrow \sigma_{Sb-X}$*, π_{PhCN}*
				0.167	HOMO	LUMO+4	$\pi_C, \pi_{PhOMe} \rightarrow \sigma_{Sb-X}$*, π_{PhCN}*
6	25557.4	391.3	1.750	0.564	HOMO-2	LUMO+1	$\pi_C \rightarrow \pi_C$*
7	26648.0	375.3	1.021	0.220	HOMO-2	LUMO	$\pi_C \rightarrow \pi_C$*
				0.159	HOMO-1	LUMO+1	$\pi_C, \pi_{PhOMe} \rightarrow \pi_C$*
				0.144	HOMO	LUMO+1	$\pi_C, \pi_{PhOMe} \rightarrow \pi_C$*
				0.328	HOMO	LUMO+2	$\pi_C, \pi_{PhOMe} \rightarrow \sigma_{Sb-X}$*, π_{PhCN}*
8	28067.9	356.3	0.367	0.620	HOMO-2	LUMO+2	$\pi_C \rightarrow \sigma_{Sb-X}$*, π_{PhCN}*
				0.158	HOMO-2	LUMO+4	$\pi_C \rightarrow \sigma_{Sb-X}$*, π_{PhCN}*
9	28425.6	351.8	0.018	0.983	HOMO-3	LUMO	$\pi_{PhOMe} \rightarrow \pi_C$*
10	29190.4	342.6	0.011	0.614	HOMO-1	LUMO+2	$\pi_C, \pi_{PhOMe} \rightarrow \sigma_{Sb-X}$*, π_{PhCN}*
				0.172	HOMO	LUMO+2	$\pi_C, \pi_{PhOMe} \rightarrow \sigma_{Sb-X}$*, π_{PhCN}*
11	29468.5	339.3	0.229	0.111	HOMO-1	LUMO+4	$\pi_C, \pi_{PhOMe} \rightarrow \sigma_{Sb-X}$*, π_{PhCN}*
				0.129	HOMO	LUMO+2	$\pi_C, \pi_{PhOMe} \rightarrow \sigma_{Sb-X}$*, π_{PhCN}*
				0.617	HOMO	LUMO+4	$\pi_C, \pi_{PhOMe} \rightarrow \sigma_{Sb-X}$*, π_{PhCN}*

C = Corrole ring, PhOMe = Trimethoxyphenyl ring, PhCN = Cyanophenyl rings, Sb-X = Antimony-halide bonds

9 References

1   B. Durham, J. V. Caspar, J. K. Nagle and T. J. Meyer, *JACS*, 1982, **104**, 4803-4810.
2   J. N. Demas and G. A. Crosby, *Phys. Chem.*, 1971, **48**, 991-1024.
3   P. R. Ogibly and C. S. Foote, *J. Am. Chem. Soc.*, 1983, **105**, 3423-3430.
4   R. Schmidt, C. Tanielian, R. Dunsbach and C. Wolff, *J. Photochem. Photobiol. A*, 1994, **79**, 11-17.
5   N. Epelde-Elezcano V. Martínez-Martínez, E. Peña-Cabrera, C. F. A. Gómez-Durán, I. L. Arbeloa and S. Lacombe, *RSC Adv.*, 2016, **6**, 41991-41998
6   F. Neese, *WIREs Comput Mol Sci*, 2012, **2**, 73–78; F. Neese, *WIREs Comput Mol Sci*, 2018, **8**, e1327; F. Neese, F. Wennmohs, U. Becker and C. Riplinger, *J. Chem. Phys.*, 2020, **152**, 224108
7   Y. Zhao and D. G. Truhlar, *Theor Chem Account*, 2008, **120**, 215–241; B. Metz, H. Stoll and M. Dolg, *J. Chem. Phys.*, 2000, **113**, 2563-2569; F. Weigend and R. Ahlrichs, *Phys. Chem. Chem. Phys.*, 2005, **7**, 3297-3305.
8   S. Grimme, J. Antony, S. Ehrlich and H. Krieg, *J. Chem. Phys.*, 2010, **132**, 154104.
9   F. Neese, *J. Comput. Chem.*, 2003, **24**, 1740-1747; F. Weigend, *Phys. Chem. Chem. Phys.*, 2006, **8**, 1057-1065; F. Neese, F. Wennmohs, A. Hansen and U. Becker, *Chem. Phys.*, 2009, **356**, 98-109; R. Izsák and F. Neese, *J. Chem. Phys.*, 2011, **135**, 144105.
10 M. Garcia-Ratés and F. Neese, *J. Comput. Chem.*, 2020, **41,** 922-939.
11 D. Bykov, T. Petrenko, R. Izsák, S. Kossmann, U. Becker, E. Valeev and F. Neese, *Molecular Physics*, 2015, **113**, 1961-1977; M. Garcia-Ratés and F. Neese, *J. Comput. Chem.*, 2019, **40**, 1816-1828.
12 F. Neese and G. Olbrich, *Chem. Phys. Lett.*, 2002, **362**, 170-178; T. Petrenko, S. Kossmann and F. Neese, *J. Chem. Phys.*, 2011, **134**, 054116.
13 E. C. Meng, T. D. Goddard, E. F. Pettersen, G. S. Couch, Z. J. Pearson, J. H. Morris and T. E. Ferrin, Protein Sci., 2023, **32**, e4792; T. D. Goddard, C. C. Huang, E. C. Meng, E. F. Pettersen, G. S. Couch, J. H. Morris and T. E. Ferrin, *Protein Sci.*, 2018, **27**, 14-25; A. J. Schaefer, V. M. Ingman and S. E. Wheeler, *J. Comput. Chem.*, 2021, **42**, 1750-1754; V. M. Ingman, A. J. Schaefer, L. R. Andreola and S. E. Wheeler, *WIREs Comput Mol Sci.*, 2021, **11**, e1510.